Impacts of Ocean Cooling and Reduced Wind Drag on Hurricane Katrina (2005) Based on Numerical Simulations

YINGJIAN CHEN

State Key Laboratory of Hydroscience and Engineering, Department of Hydraulic Engineering, Tsinghua University, Beijing, China, and Department of Meteorology and Atmospheric Science, and Center for Advanced Data Assimilation and Predictability Techniques, The Pennsylvania State University, University Park, Pennsylvania

FUQING ZHANG

Department of Meteorology and Atmospheric Science, and Center for Advanced Data Assimilation and Predictability Techniques, The Pennsylvania State University, University Park, Pennsylvania

BENJAMIN W. GREEN

University of Colorado Boulder, Cooperative Institute for Research in Environmental Sciences, and NOAA/Earth System Research Laboratory/Global Systems Division, Boulder, Colorado

XIPING YU

State Key Laboratory of Hydroscience and Engineering, Department of Hydraulic Engineering, Tsinghua University, Beijing, China

(Manuscript received 13 June 2017, in final form 7 November 2017)

ABSTRACT

Tropical cyclone (TC) intensity is strongly influenced by surface fluxes of momentum and moist enthalpy (typically parameterized in terms of "exchange coefficients" C_d and C_k, respectively). The behavior of C_d and C_k remains quite uncertain especially in high wind conditions over the ocean; moreover, moist enthalpy flux is extremely sensitive to sea surface temperature (SST). This study focuses on numerical simulations of Hurricane Katrina (2005) from an atmosphere–ocean coupled modeling system to examine the combined impacts of air–sea flux parameterizations and ocean cooling on TC evolution. Three momentum flux options—which make C_d increase, level off, or decrease at hurricane-force wind speeds—with five different C_k curves are tested. Maximum 10-m wind speed V_{max} is highly sensitive to C_d, with weaker sensitivities for minimum sea level pressure P_{min} and track. Atmosphere-only runs that held SST fixed yielded TCs with P_{min} substantially deeper than observations. Introducing ocean coupling weakens TC intensity with much more realistic P_{min}. The coupled run with the flux parameterization that decreases C_d at high wind speeds yields a simulated TC intensity most consistent with observations. This C_d parameterization produces TCs with the highest V_{max}. Increasing C_k generally increases surface heat fluxes and thus TC intensity. For coupled runs using the default C_k parameterization, the simulated SST fields are similar (regardless of C_d parameterization) and agree well with satellite observations. The mesoscale oceanic eddies, which are well resolved in the ocean model, contribute to the magnitude of TC-induced SST cooling and greatly influence TC intensity.

1. Introduction

Tropical cyclones (TCs), especially hurricanes or typhoons, are often disastrous once they make landfall. Strong winds and massive storm surge generated by TCs have the potential to cause severe human and economic losses. To minimize these losses, accurate forecasts of TC track, intensity, and surge are necessary several days in advance. Although forecast errors of TC track have been greatly reduced over the past two and a half decades, predicting TC intensity remains quite difficult

Corresponding authors: Fuqing Zhang, fzhang@psu.edu; Xiping Yu, yuxiping@tsinghua.edu.cn

DOI: 10.1175/MWR-D-17-0170.1

(Rappaport et al. 2009); this is at least partly attributable to an incomplete understanding and poor parameterization of inner-core dynamics and small-scale processes (e.g., Chen et al. 2007; Zhang and Weng 2015).

Among many factors, fluxes of momentum τ and moist enthalpy H at the air–sea interface are believed to be crucial in determining TC intensity. They can be expressed as

$$\tau = \rho_a C_d U^2, \quad (1)$$

$$H = \rho_a C_k U(k_s^* - k_a), \quad (2)$$

respectively, where ρ_a is the air density; U is the wind speed at a reference height (usually 10 m); C_d and C_k are the exchange coefficients for drag (momentum) and enthalpy, respectively; k_s^* is the saturation enthalpy at the sea surface; and k_a is the enthalpy of the near-surface air. Both theoretical (e.g., Emanuel 1995) and numerical (e.g., Bryan 2012; Green and Zhang 2013, 2014; Zhang and Emanuel 2016) analyses have reported that the maximum 10-m wind speed $V_{\max}$ and minimum sea level pressure (SLP) $P_{\min}$ are sensitive to C_d and C_k. For example, the well-known potential intensity theory of Emanuel (1995) states that $V_{\max}$ ($P_{\min}$) of a mature TC increases (decreases) with the ratio C_k/C_d. Therefore, it is of critical importance to accurately represent these two exchange coefficients in TC modeling.

Unfortunately, the exact behavior of C_d over the ocean under strong, hurricane-force winds remains an open science question. Because few direct measurements of the TC surface layer over open waters were available decades ago, it was long assumed that C_d over the ocean increases monotonically with increasing wind speed. More recent studies, however, found that C_d appears to level off (e.g., Donelan et al. 2004) or decrease (e.g., Powell et al. 2003; Jarosz et al. 2007; Holthuijsen et al. 2012) for wind speeds above $\sim 33\,\mathrm{m\,s^{-1}}$. Theoretically, Donelan et al. (2004) considered the saturated C_d as a result of flow separation due to continuous wave breaking. Other studies that supported the reduced C_d attributed such behavior to the impact of sea spray generated by breaking waves. The suspended spray influences the atmospheric boundary layer flow through 1) directly interacting with the momentum of the near-surface air (e.g., Andreas 2004; Kudryavtsev and Makin 2011) or 2) dissipating additional turbulent kinetic energy because of the density stratification of spray, which is similar to the effect of stably stratified temperature on the airflow (e.g., Kudryavtsev 2006; Chen and Yu 2016). Parameterization schemes that make C_d saturate with wind speed are currently predominant in TC numerical models, but the use of reduced C_d has started to appear in recent years (e.g., Zweers et al. 2010, 2015; Tallapragada et al. 2015).

Recently, Green and Zhang (2013, 2014) investigated the impacts of different surface flux parameterizations on the characteristics of simulated TCs. But their results were far from conclusive because the feedback between strong near-surface winds and sea surface temperature (SST) was not taken into account. It is well known that SST cools under hurricane wind forcing, primarily due to the vertical shear-driven entrainment of the colder thermocline water (Price 1981) and ocean-current-induced advection (Chen et al. 2010). This cooling effect results in a negative feedback process that can reduce the enthalpy flux and impede TCs from additional intensification (Chen et al. 2010; Zambon et al. 2014).

The main goal of the present study is to expand upon the work of Green and Zhang (2013, 2014) in evaluating the impacts of different air–sea flux parameterizations on TC intensity and structure, but in a coupled atmosphere–ocean framework [rather than the atmosphere-only uncoupled simulations used by Green and Zhang (2013, 2014)]. This is an important step to see if the results of Green and Zhang (2013, 2014) remain valid when the interaction with the ocean (particularly, the important feedback process of SST cooling) is considered. Additionally, this study will also test implementation of the Chen and Yu (2016, 2017) parameterization for momentum flux (see section 2) that attempts to account for the impact of suspended sea spray on the air–sea momentum transfer. The Coupled Ocean–Atmosphere–Wave–Sediment Transport (COAWST) modeling system (Warner et al. 2010) is used here to numerically simulate TCs. COAWST couples the atmospheric Weather Research and Forecasting (WRF) Model (Skamarock et al. 2008) with the three-dimensional Regional Oceanic Modeling System (ROMS; Shchepetkin and McWilliams 2005). Compared to empirically based SST cooling algorithms (Kilic and Raible 2013; Zweers et al. 2015) or one-dimensional mixed-layer modeling (Davis et al. 2008; Halliwell et al. 2015), a three-dimensional model like ROMS is expected to have the ability to fully resolve the ocean response (including the cold-wake structure) to hurricane forcing (Chen et al. 2010). Three momentum flux options (which have distinct behaviors of C_d in high wind conditions)—each of which are tested with five different amplitudes of the corresponding C_k curves—are chosen to implement our goals through atmospheric-convection-permitting, air–sea-coupled, COAWST simulations of Hurricane Katrina (2005).

The remainder of the paper is organized as follows. Section 2 provides a brief review of the surface flux parameterization schemes used in this study. Section 3 describes the coupled model and details the

experimental setup. Numerical results are presented and analyzed in section 4. Conclusions are given in section 5.

2. Description of surface flux schemes

a. Drag coefficient

The wind drag coefficient C_d over the sea surface is far from a simple parameter that can be easily determined. In reality, C_d is a function of wind speed, atmospheric stability, and sea state (i.e., surface wave characteristics). For the sake of practicality, most scientific research and operational TC models parameterized C_d under neutral stability as a function of the 10-m wind speed u_{10} (e.g., Garratt 1977; Large and Pond 1981; Wu 1982). Other, more recent, schemes have parameterized momentum flux in terms of the aerodynamic roughness length z_0 [which, over the ocean, is strongly dependent on wind forcing (i.e., u_{10})]; under neutral stability, C_d can be related to z_0 via

$$C_d = \left[\frac{\kappa}{\ln(z_{\rm ref}/z_0)}\right]^2, \tag{3}$$

where κ is the von Kármán constant and $z_{\rm ref}$ is a reference height (often 10 m) in the surface layer. In this study, three parameterization options for C_d are considered as follows.

1) WRF2

This scheme was developed after the experiments conducted by Donelan et al. (2004) showed that C_d levels off at hurricane wind speeds. The scheme was first implemented in version 3.0 of the Advanced Research core of WRF (WRF-ARW) and then further modified in version 3.4.1. This option can be used in WRF by setting isftcflx = 2 in the model's namelist file. The momentum roughness length z_0 in this scheme is given by

$$z_0 = \max\{1.27\times10^{-7}, \min[z_w z_2 + (1-z_w)z_1, 2.85\times10^{-3}]\}, \tag{4a}$$

$$z_w = \min\left[1, \left(\frac{u_*}{1.06}\right)^{0.3}\right], \tag{4b}$$

$$z_1 = 0.011\frac{u_*^2}{g} + 1.59\times10^{-5}, \tag{4c}$$

$$z_2 = \frac{10}{\exp(9.5u_*^{-1/3})} + \frac{1.65\times10^{-6}}{\max(u_*, 0.01)}, \tag{4d}$$

where u_* is the friction velocity and g is the acceleration due to gravity. Note that under the assumption of neutral stability, z_0 can be related back to C_d via (3).

2) GZ13

Green and Zhang (2013) took an ad hoc approach that used (4) to parameterize z_0 at low wind speeds but allowed for a continued increase in z_0 at wind speeds above $\sim$33 m s^{-1} [i.e., removing the upper limit of $z_0 = 2.85\times10^{-3}$ m shown in (4) above, cf. their (13)]:

$$z_{0,\rm GZ13} = \begin{cases} z_0, & |z_0 \le 2.85\times10^{-3} \\ \dfrac{z_0 - 2.85\times10^{-3}}{2} + 2.85\times10^{-3}, & |z_0 > 2.85\times10^{-3} \end{cases}. \tag{5}$$

Different from Green and Zhang (2013)—which as noted above uses (4) as an input into (5)—the present study uses the formulation of z_0 given by isftcflx = 2 *in version 3.3.1* of WRF-ARW:

$$z_0 = \max\left[1.27\times10^{-7}, \frac{10}{\exp(9.5u_*^{-1/3})} + \frac{1.65\times10^{-6}}{\max(u_*, 0.01)}\right], \tag{6}$$

as the input into (5). In other words, the "GZ13" parameterization used in this study is a combination of (5) and (6).

This parameterization scheme is used in the WRF-based ensemble Kalman filter (EnKF) real-time Atlantic TC prediction system run at The Pennsylvania State University (PSU) (http://hfip.psu.edu/realtime). We tested the GZ13-like parameterizations based on version 3.3.1 [used in this manuscript and in the above-mentioned real-time system, as (5) and (6)] and version 3.4.1 [used by Green and Zhang (2013), as (4) and (5)]; the impacts of this minor difference in flux parameterization on simulated TC intensity were negligible (not shown).

3) CY16

Recently, Chen and Yu (2016, 2017) extended the atmospheric wave boundary layer model (WBLM; e.g., Moon et al. 2004)—which is used to calculate wind stress at a wavy ocean surface—to take into account the additional energy dissipation due to the stable stratification of suspended sea spray. Their enhanced WBLM yields a decreasing tendency in C_d at hurricane-force wind speeds and the results showed a fairly good agreement with the field measurements published by Powell et al. (2003), Jarosz et al. (2007), and Holthuijsen et al. (2012). For simplicity, we omit the effect of wave variability on the surface momentum flux in this study and thus we fit a second-order polynomial to the numerical data [cyan dots in Fig. 4 of Chen and Yu (2017)] in order to obtain C_d as a function of u_{10} only. The fitted curve is written as

$$C_d = [\max(5, -0.014u_{10}^2 + 1.033u_{10} + 4.895)] \times 10^{-4}. \quad (7)$$

The lower limit of C_d is added in order to avoid a too small or even negative value when u_{10} increases beyond $\sim 73\,\mathrm{m\,s^{-1}}$.

Figure 1a plots C_d as a function of u_{10} for the above three momentum flux parameterizations. Although all three C_d curves increase monotonically at moderate wind speeds and reach similar values at $u_{10} \approx 33\,\mathrm{m\,s^{-1}}$, they behave quite differently at higher hurricane-force wind speeds. It is therefore expected that the simulated 10-m wind fields will differ significantly between the experiments with different C_d parameterizations.

b. Moist enthalpy coefficient

The moist enthalpy flux is the sum of the sensible heat H_S and latent heat fluxes H_L. They can be expressed as

$$H_S = \rho_a c_p C_h u_{10} \Delta\theta, \quad (8)$$

$$H_L = \rho_a L_v C_q u_{10} \Delta q, \quad (9)$$

where c_p is the specific heat capacity of air; L_v is the latent heat of vaporization; C_h and C_q are the exchange coefficients for sensible and latent heat, respectively; and $\Delta\theta$ and Δq are the differences of potential temperature and humidity between air and sea, respectively. In this study, the treatment of C_h and C_q is based on namelist option isftcflx = 2 in version 3.4.1 of WRF-ARW. These formulas originate from Brutsaert (1975), and can be written as follows [cf. (6) and (7) of Green and Zhang (2014)]:

$$C_h = \frac{C_d}{1 + \beta^{-1} C_d^{1/2} (7.3 \mathrm{Re}_*^{1/4} \mathrm{Pr}^{1/2} - 5)}, \quad (10)$$

$$C_q = \frac{C_d}{1 + \beta^{-1} C_d^{1/2} (7.3 \mathrm{Re}_*^{1/4} \mathrm{Sc}^{1/2} - 5)}, \quad (11)$$

where Pr = 0.71 and Sc = 0.60 are Prandtl and Schmidt numbers, respectively (Garratt 1992); and $\mathrm{Re}_* = u_* z_0 / \nu$ is the roughness Reynolds number with kinematic viscosity of air ν. Since C_h and C_q have received comparatively less attention than C_d, they are also uncertain and still poorly parameterized. Following Green and Zhang (2014), a tunable parameter β is added in (10) and (11) to further examine the sensitivity of hurricane intensity to the parametric uncertainty in air–sea heat exchange. It can be inferred that β has a direct effect on C_h and C_q, that is, increasing β increases both heat exchange coefficients. In this study, β is tested with values of 0.5, 0.75, 1.0, 1.5, and 2.0. Note that the scheme with $\beta = 1.0$ is the same as in version 3.4.1 of WRF-ARW.

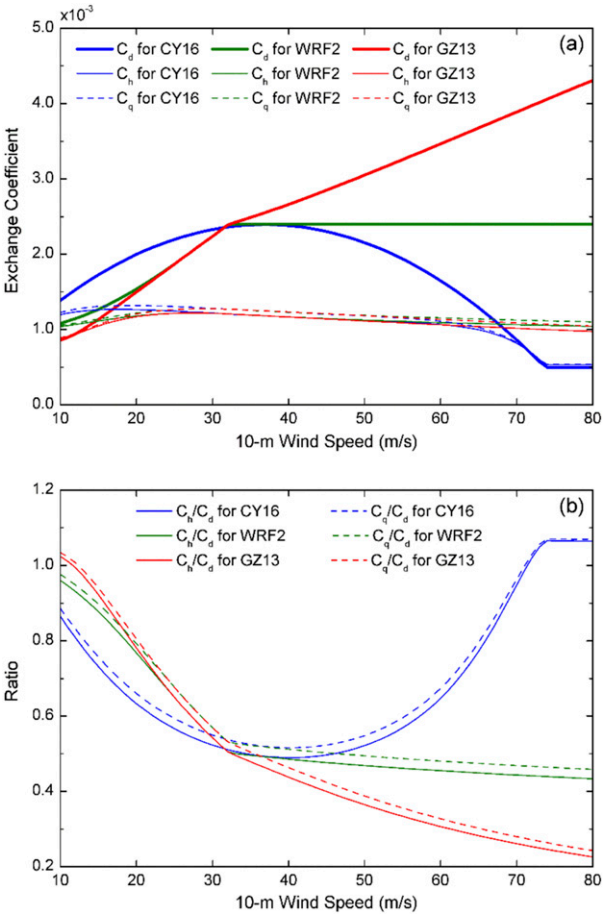

FIG. 1. Plots as functions of 10-m wind speed of (a) exchange coefficients for drag C_d, sensible heat C_h, and latent heat C_q (for both C_h and C_q, $\beta = 1.0$); and (b) exchange coefficient ratios C_h/C_d (solid) and C_q/C_d (dashed) for each of the three flux parameterizations: CY16 (blue), WRF2 (green), and GZ13 (red).

Figure 1a also plots C_h and C_q as functions of u_{10} when $\beta = 1.0$. Although the three flux options all use the same formulas for C_h and for C_q, the *values* of these exchange coefficients differ slightly—particularly in extremely strong wind conditions ($u_{10} > 70\,\mathrm{m\,s^{-1}}$)—because of their dependence on C_d [cf. (10) and (11)]. Additionally, the resulting C_h and C_q curves within each flux option are close to each other, with $C_q > C_h$.

c. Exchange coefficient ratio

The exchange coefficient ratio C_k/C_d is considered to be an important factor in the minimum sea level pressure and maximum near-surface wind speed of a mature TC (e.g., Emanuel 1995; Green and Zhang 2013; Zhang and Emanuel 2016). Figure 1b shows the ratios C_h/C_d and C_q/C_d resulting from the three flux schemes when $\beta = 1.0$ (because C_h/C_d and C_q/C_d are so close, either one can be considered as a reasonable approximation for C_k/C_d). Both options WRF2

and GZ13 yield ever-decreasing ratios with increasing wind speeds. On the contrary, the ratios for option CY16 decrease at first and then increase. Because the change of β changes C_k but has no impact on C_d, increasing β increases the exchange coefficient ratios for all flux schemes.

3. Model configuration and experimental design

Following Green and Zhang (2013), the present work is focused on Hurricane Katrina. Katrina tracked through the Gulf of Mexico in late August 2005, reaching its peak intensity of maximum 10-m wind speed V_{max} = 150 kt (77.2 m s^{-1}) and minimum sea level pressure P_{min} = 902 hPa. The hurricane made landfalls in Louisiana and Mississippi, causing over 5 m in storm surge in many locations and more than 1800 deaths (Knabb et al. 2006). Such an extremely intense hurricane provides a great opportunity to examine the impacts on simulated TCs of various parameterizations of C_d and C_k in high wind conditions over water.

The coupled modeling system used here is COAWST, version 3.2. COAWST comprises several state-of-the-art component numerical models, including for the atmosphere (WRF-ARW), ocean (ROMS), sea surface waves [Simulating Waves Nearshore (SWAN); Booij et al. 1999], sediment [Community Sediment Transport Modeling System (CSTMS); Warner et al. 2008], and sea ice. The Model Coupling Toolkit (MCT; Larson et al. 2005) acts as the coupler to exchange data fields between the component models.

In this study, we use COAWST in two modes: uncoupled atmosphere (WRF) only, and coupled atmosphere–ocean (WRF + ROMS). While it is generally accepted that surface momentum flux over the ocean is affected by the surface waves (e.g., Donelan et al. 1993; Taylor and Yelland 2001), a detailed examination of this effect on the TC simulations is beyond the scope of the present research. Therefore, none of our simulations include coupling to a wave model (SWAN); it should be noted that many research and operational TC models do not include wave coupling. Brief descriptions of each model component and configuration are given below.

a. Atmospheric model

WRF is an atmospheric numerical weather prediction model designed for both meteorological research and operational applications (Skamarock et al. 2008). It solves the Euler nonhydrostatic and fully compressible equations and features a multitude of different options for parameterizing subgrid-scale processes. Numerous studies have used WRF for TC research and forecasting purposes. In the COAWST framework of this study, all simulations of the atmosphere were run using WRF-ARW, version 3.7.1.

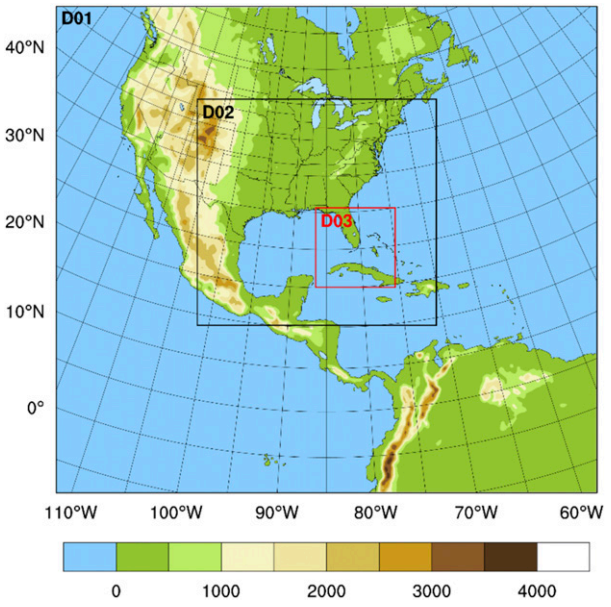

FIG. 2. Configuration of WRF domains. The red box represents the initial position of the vortex-following nest D03. Color shading denotes topography in meters.

There were three domains in the present work—D01, D02, and D03 (Fig. 2)—with horizontal grid spacings of 27, 9, and 3 km with corresponding dynamic time steps of 60, 20, and 20/3 s, respectively. A total of 43 vertical levels with a pressure top of 5 hPa were used. While the outer two domains (D01 and D02) were fixed in space throughout the simulations, D03 was set to be vortex following. A significant upgrade in version 3.2 of COAWST is that a moving WRF nest can be configured in the atmosphere–ocean coupled runs. This new feature makes it possible to better resolve the dynamics of the TC inner core at significantly reduced computational cost.

The atmospheric initial conditions were derived from Green and Zhang (2013). They first created an ensemble of 60 forecast members at 0000 UTC 25 August 2005. After 14.5 h of spinup to create a flow-dependent covariance matrix, the EnKF data assimilation technique—which has been shown to significantly improve forecasts of TC position and intensity (Weng and Zhang 2012; Zhang and Weng 2015; Weng and Zhang 2016)—was used to assimilate airborne Doppler radar velocity data over six cycles from 1430 to 2000 UTC 25 August. The ensemble mean analysis at 2000 UTC was integrated forward an additional 4 h to 0000 UTC 26 August 2005; this deterministic forecast served as the atmospheric initial conditions for this study (as in Green and Zhang 2013, 2014). The atmospheric lateral boundary conditions throughout the integration period were obtained from the operational Global Forecast System (GFS) initialized at 0000 UTC 25 August 2005. The

sensitivity of the simulations to changes in surface flux parameterization and ocean coupling during the assimilation stage is beyond the scope of the present paper.

The physics options used in WRF were nearly identical to those of Green and Zhang (2013). The Grell–Devenyi cumulus scheme (Grell and Devenyi 2002) was implemented for D01, while both D02 and D03 used explicitly resolved convection. Also used were the WRF single-moment 6-class (with graupel) microphysics scheme (Hong and Lim 2006), the Rapid Radiative Transfer Model for longwave radiation (Mlawer et al. 1997), and the Dudhia (1989) shortwave radiation scheme. The Yonsei University (YSU) planetary boundary layer scheme (Hong et al. 2006) was employed with "MM5 similarity" (sf_sfclay_physics option 91 in WRF V3.7.1) and five-layer thermal diffusion over land.

It should be noted that a "dissipative heating" term in the surface layer physics was introduced into WRF-ARW, but removed in V3.6.1 [i.e., *after* the studies of Green and Zhang (2013, 2014)]. The idea behind dissipative heating is that all energy loss at the surface is converted into internal heat. In reality, much of the energy lost at the surface in a TC over water is transferred to surface waves and the underlying ocean. So, for atmosphere–ocean coupled modeling (even without a surface wave model), a dissipative heating term may not be always desirable. Moreover, by passing surface stress from the atmosphere to the ocean during coupling (see section 3c below), the implication is that all surface energy loss is transferred directly to the ocean (rather than converted to internal heat). Thus, including dissipative heating within an atmosphere–ocean coupled model could introduce a spurious surface energy source. Unfortunately, we only became aware of this issue after running the simulations—all of which included dissipative heating in an attempt to be as consistent as possible with the work of Green and Zhang (2013, 2014). Computational limitations prevented a rerunning of all experiments (coupled and uncoupled) *without* dissipative heating in the current study, but will be considered in future studies.

b. Ocean model

ROMS is a split-explicit, free-surface, topography-following-coordinate ocean model (Shchepetkin and McWilliams 2005). This model solves the three-dimensional Reynolds-averaged Navier–Stokes equations with the hydrostatic and Boussinesq approximations. It also solves the nonlinear equation of state for seawater density and solves the conservative transport equations for temperature and salinity. Several researchers have utilized ROMS to investigate the ocean response to TC wind forcing (e.g., Seo and Xie 2013; Mei et al. 2015; Glenn et al. 2016; Seroka et al. 2016).

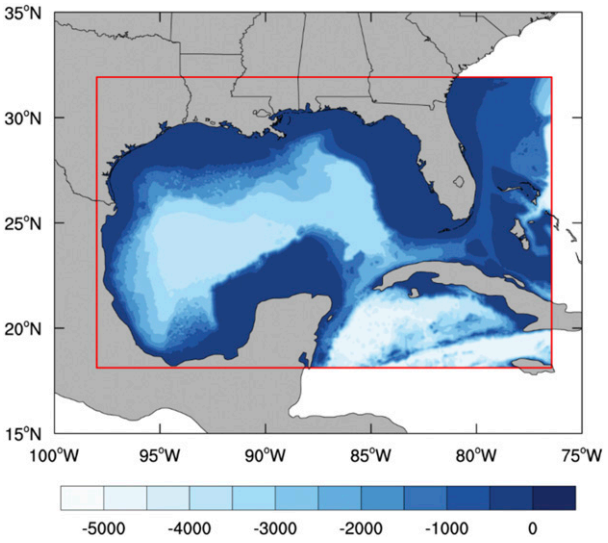

FIG. 3. ROMS domain configuration (red box). The shades of blue denote the bathymetry in meters.

In this paper, only one computational domain with a horizontal grid spacing of 1/25° (~4 km) was adopted for the ROMS component. It covers the entire Gulf of Mexico and the southern part of the U.S. Atlantic coast (Fig. 3). Although the ROMS domain is smaller than WRF D01, it does provide complete coverage of the areas that Katrina passed through and is thus sufficiently large for the purposes of capturing the coupled air–sea interaction related to the TC. The model was configured to have 36 stretched terrain-following vertical levels with at least 15 of these in the upper 50 m (the vertical stretching parameters are $\theta_s = 9$, $\theta_b = 0$, and $T_{\text{cline}} = 50$) in order to better resolve the ocean mixed layer. The ocean bathymetry was derived from the General Bathymetric Chart of the Oceans (GEBCO), which has a global 30 arc-s interval grid (http://www.gebco.net/). A baroclinic time step of 30 s was used.

The initial and lateral boundary conditions of sea level, currents, temperature, and salinity necessary to run ROMS were all obtained from Hybrid Coordinate Ocean Model with Naval Research Laboratory Coupled Ocean Data Assimilation (HYCOM + NCODA) Global 1/12° Reanalysis (http://hycom.org/data/glbu0pt08/expt-19pt1). HYCOM + NCODA assimilates available satellite altimeter observations, satellite and in situ SSTs, as well as available in situ vertical temperature and salinity profiles from XBTs, Argo floats, and moored buoys.

We followed Zambon et al. (2014), whereby the mixed radiation-nudging boundary condition was adopted with a time scale of 1 day on inflow and 10 days on outflow to pass HYCOM + NCODA temperature, salinity, and the 3D current fields to ROMS. Chapman (1985), Flather (1976), and gradient boundary conditions were imposed in the open boundary for free surface level, two-dimensional

TABLE 1. Case list for Hurricane Katrina (2005).

Case ID	Case name	WRF	ROMS	Momentum flux option	β in (10) and (11)
1	CY16_A	Yes	No	CY16	1.0
2	WRF2_A			WRF2	
3	GZ13_A			GZ13	
4	CY16_C	Yes	Yes	CY16	1.0
5	WRF2_C			WRF2	
6	GZ13_C			GZ13	
7	CY16_C_0.5	Yes	Yes	CY16	0.5
8	CY16_C_0.75				0.75
9	CY16_C_1.5				1.5
10	CY16_C_2.0				2.0
11	WRF2_C_0.5	Yes	Yes	WRF2	0.5
12	WRF2_C_0.75				0.75
13	WRF2_C_1.5				1.5
14	WRF2_C_2.0				2.0
15	GZ13_C_0.5	Yes	Yes	GZ13	0.5
16	GZ13_C_0.75				0.75
17	GZ13_C_1.5				1.5
18	GZ13_C_2.0				2.0

momentum, and mixing turbulent kinetic energy, respectively. The generic length scale method with the k–ε closure scheme (Warner et al. 2005) was implemented for parameterization of the ocean vertical turbulent mixing. In addition, the surface momentum and heat fluxes were computed in WRF and directly passed to ROMS. This approach ensures consistent flux calculations between WRF and ROMS (Zambon et al. 2014) and is necessary for a coupled model because fluxes could differ significantly (e.g., in TC cases) if they are computed separately in the two component models.

c. Model coupling

COAWST allows the transmission and transformation of prognostic variables between various component models using MCT (Larson et al. 2005). While WRF received SST from ROMS, it provided ROMS with wind stress (i.e., momentum flux), shortwave/longwave radiation, sensible/latent heat flux, and sea level pressure. Because the variables were exchanged on different grids, the Spherical Coordinate Remapping Interpolation Package (SCRIP; Jones 1998) was used to implement a conservative remapping scheme and compute the interpolation weights. The coupling interval was set to 900 s in this study. This interval is shorter than the 3600- and 1200-s intervals used in Warner et al. (2010) and Olabarrieta et al. (2012), respectively. An even smaller coupling interval of 300 s was tested, with negligible impact (not shown). Therefore, the 900-s coupling interval is likely short enough to capture the key physical processes involved in TC-related air–sea interaction, with the added benefit of reduced computational costs (as compared to a 300-s coupling interval).

d. Descriptions of the experiments

As listed in Table 1, a set of 18 experiments were carried out to investigate the combined impacts of ocean coupling (which can capture SST cooling) and air–sea flux parameterizations on Katrina's intensity and structure:

Cases 1–3 (GZ13_A, WRF2_A, and CY16_A) were atmosphere-only WRF runs not coupled to ROMS. The SST field, which also originated from global HYCOM reanalysis, was forced to be fixed in time. Cases 4–6 (GZ13_C, WRF2_C, and CY16_C) were atmosphere–ocean coupled WRF + ROMS runs. As indicated by their names, each of the three cases in either group (uncoupled or coupled) used one of the three different options described in section 2a to parameterize momentum flux. For all of these first six cases, β was set to 1.0, that is, they all used the same enthalpy flux scheme [namelist option isftcflx = 2 in version 3.4.1 of WRF-ARW, see (10) and (11) above]. Cases 7–18 were similar to cases 4–6, except that different values of β (0.5, 0.75, 1.5, or 2.0) were used to further examine the impact of C_k uncertainty on the numerical results.

For all experiments, both atmosphere and ocean models were initialized at 0000 UTC 26 August 2005, before Katrina moved into the Gulf of Mexico. The runs were integrated forward 5 days to 0000 UTC 31 August 2005.

4. Results and analysis

a. Ocean initial conditions

Figure 4 plots the initial conditions (from HYCOM) of ocean temperature at sea surface (i.e., SST) and at 50-m depth. The HYCOM-derived SST was over 30°C

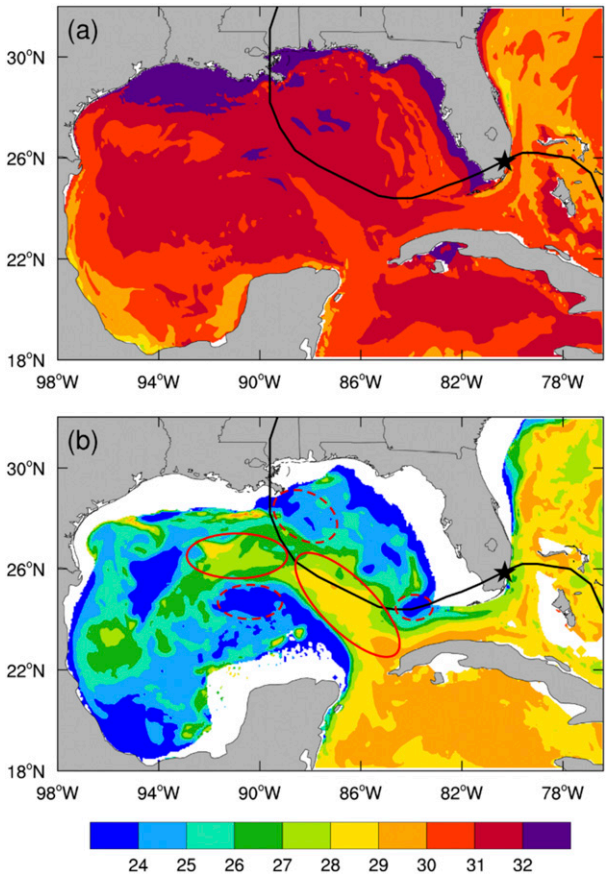

FIG. 4. HYCOM-derived initial conditions for ocean temperature (°C) at (a) sea surface (i.e., SST) and (b) 50-m depth at 0000 UTC 26 Aug 2005. The black line denotes the observed best track of Hurricane Katrina, with the star indicating the TC's position at the initial time. The solid (dashed) red ovals denote warm (cold) core eddies.

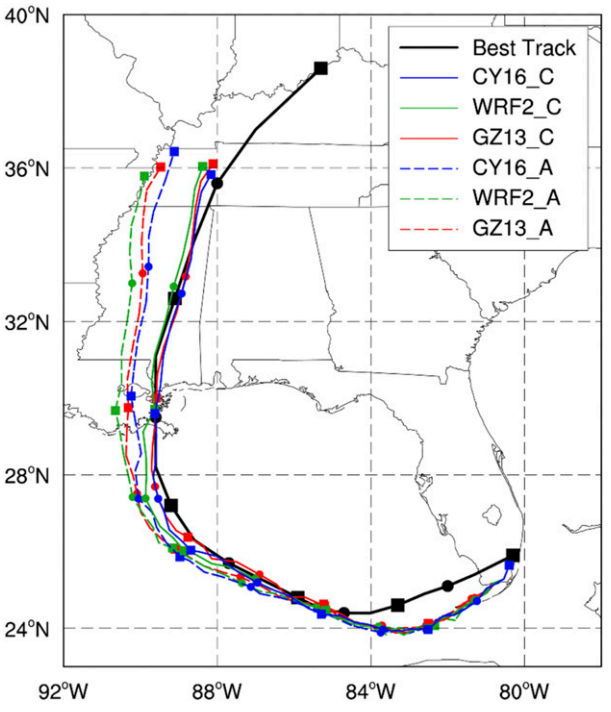

FIG. 5. Comparison of Katrina's best track (black) and six simulated tracks (cases 1–6 in Table 1, all with $\beta = 1.0$) between 0000 UTC 26 Aug and 0000 UTC 31 Aug 2005. Positions at 0000 (1200) UTC are marked by squares (circles).

across almost the entirety of the Gulf of Mexico before the hurricane traversed it; such warm SSTs are considered to be favorable for TC development and intensification. Warm core eddies (including the Loop Current) and cold core eddies are also evident in Fig. 4. As stated by Jaimes and Shay (2009), the dependence of TC-induced oceanic cooling on the presence of these mesoscale eddies is a critical issue for intensity change of TCs in the Gulf of Mexico. However, such mesoscale variability cannot be captured in numerical simulations if the satellite-derived nearly homogeneous SST is applied (Jaimes and Shay 2009) or the SST field is forced to be time independent.

b. Hurricane track and intensity

The tracks of Katrina simulated by cases 1–6 are plotted in Fig. 5 along with the observed best track. For these cases, the tunable parameter β in (10) and (11) is set to 1.0. As in Olabarrieta et al. (2012) and Green and Zhang (2013), the tracks are not sensitive to the parameterizations of air–sea momentum flux. This is because TC track is primarily dependent on large-scale steering flows that are less influenced by smaller-scale processes such as air–sea surface fluxes. It should be noted that there is a slight difference in track between the uncoupled and coupled runs after ~84 h (i.e., when the simulated TCs reach a latitude of ~28°N), but that determining the reasons why is beyond the scope of this paper.

Plotted in Fig. 6 are the common metrics of TC intensity—minimum SLP $P_{\min}$ and maximum 10-m wind speed $V_{\max}$—over the entire 120-h period for cases 1–6. It is clear that $V_{\max}$ is extremely sensitive to the parameterization of surface momentum flux, although $P_{\min}$ is less sensitive. This is consistent with the findings of Green and Zhang (2014) that changes to C_d at hurricane-force wind speeds (i.e., their m parameter) have statistically significant correlations with $V_{\max}$ but not with $P_{\min}$. Thus, the three momentum flux schemes used in this study yield different pressure–wind relationships, as will be shown later. The option CY16, which has the largest C_k/C_d ratio and the lowest C_d, produces the most intense TC (except for $P_{\min}$ in the uncoupled runs, where WRF2 is almost always deeper).

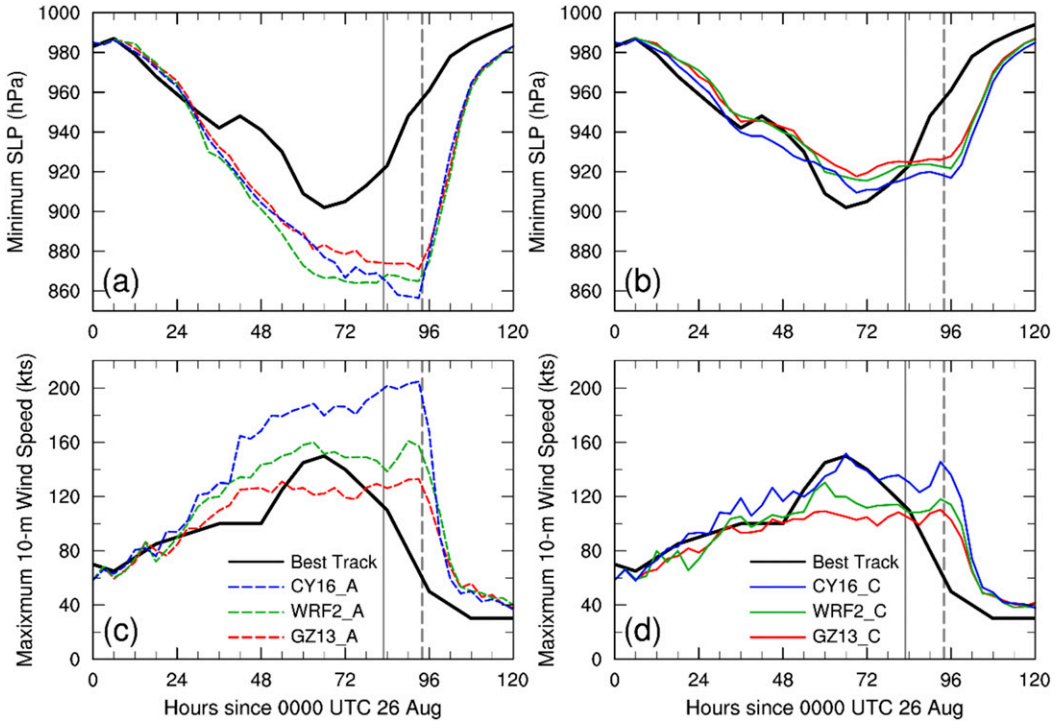

FIG. 6. Time series of Katrina's observed (black) and simulated minimum SLP for (a) uncoupled and (b) coupled experiments—cases 1–6 in Table 1, all with $\beta = 1.0$—for the 120-h period from 0000 UTC 26 Aug to 0000 UTC 31 Aug 2005. (c),(d) As in (a),(b), but for maximum 10-m wind speed. The gray solid (dashed) lines in each panel represent the time of observed (simulated) landfall.

All three uncoupled simulations (cases 1–3) yield P_{min} lower than the observed best track by over 20 hPa. While WRF2_A predicts a reasonable peak value of V_{max}, CY16_A (GZ13_A) overestimates (underestimates) the peak V_{max}. It should be noted that the results of WRF2_A and GZ13_A are similar but not identical to those in Green and Zhang (2013) as a consequence of the following experimental setup differences: the use of a newer version of WRF-ARW, a larger and static grid in D02, and the changing of the SST source. Additional experiments (not shown) suggest that changing the SST source is likely the main cause of the abovementioned differences in results between this study and Green and Zhang (2013): specifically, the GFS SSTs used in Green and Zhang (2013) were lower than the HYCOM SSTs used here.

The coupled runs (cases 4–6), which are capable of simulating SST cooling, yield significantly weaker TCs (in terms of both lower V_{max} and higher P_{min}) than the corresponding atmosphere-only uncoupled runs (cases 1–3). Of particular note is that the coupled runs—particularly CY16_C—have simulated P_{min} values much closer to the observed best track. While both WRF2_C and GZ13_C underestimate V_{max}, CY16_C has a peak V_{max} that is in good agreement with the observations. Additionally, the coupled simulations (especially CY16_C and WRF2_C) can reproduce the intensification and weakening processes during 54–78 h after the initial time; in contrast, the uncoupled runs do not experience any weakening until landfall. This implies that TC intensity can be considerably influenced by the amplitude of local SST cooling, which is predominantly controlled by the distributions of mesoscale oceanic eddies (as will be shown in section 4c), and that TC intensity cannot be accurately forecasted if SST remains static. Nevertheless, the coupled simulations are by no means perfect: there is a short reintensification period after 90 h that continues until landfall; the observed storm was slowly weakening in the time leading up to its (earlier) landfall. One possible explanation for this disagreement is that the initial condition input from HYCOM might not resolve enough bottom cold water around the area of landfall, leading to insufficient simulated SST cooling near the coast (which would favor TC strengthening). In fact, a comparison of simulated SST from CY16_C valid at 0000 UTC 30 August 2005 (a few hours after simulated landfall) with SST observations from both Tropical Rainfall Measuring Mission

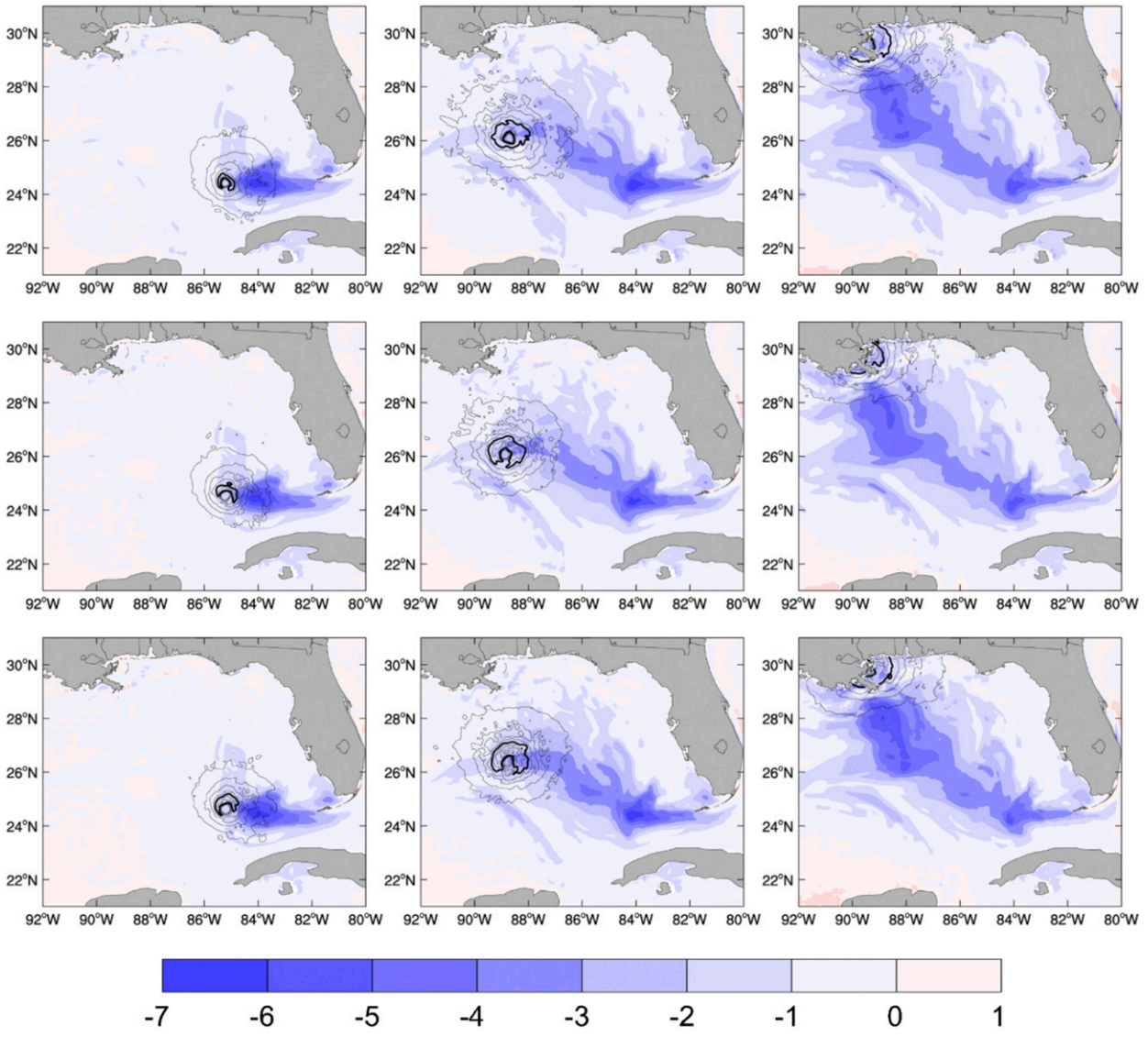

FIG. 7. Distributions of SST cooling (°C, color) and wind stress (black; thin lines every 1 N m^{-2}, thick line for 4 N m^{-2}) for the three coupled experiments: (top) CY16_C, (middle) WRF2_C, and (bottom) GZ13_C at (left) 0000 UTC 28 Aug, (center) 0000 UTC 29 Aug, and (right) 0000 UTC 30 Aug. The reference time for SST cooling is 1200 UTC 26 Aug.

(TRMM) Microwave Imager (TMI; www.remss.com/missions/tmi) and Advanced Very High Resolution Radiometer (not shown) finds that the model is more than 1°C warmer than observations right along the coast. The possibility of poor initialization for the continental shelf area was also demonstrated by Seroka et al. (2016) for the Mid-Atlantic Bight in their study of Hurricane Irene (2011). Another possible factor for the short re-intensification period is an increase in the 500-hPa relative humidity (averaged over a 300–600-km annulus from TC center) from 72 to 90 h (not shown). Deep-layer (850–200 hPa) vertical wind shear (averaged over this same annulus, also not shown) was actually increasing in the time leading up to simulated TC landfall, and thus likely did not contribute to the late intensification period.

c. *SST response*

Plotted in Fig. 7 are simulated SST cooling (relative to SST at 1200 UTC 26 August) at 0000 UTC 28, 29, and 30 August from cases 4–6 (the three coupled runs with $\beta = 1.0$). It is interesting that the evolutions in simulated SST (cooling) are similar to each other even though they are driven by hurricane-force winds of considerably different magnitudes. As mentioned above, TC-induced ocean cooling is mainly controlled by the wind stress τ.

Because GZ13_C has the largest C_d under hurricane-force winds, it outputs smaller u_{10} than the other two coupled simulations. Thus, C_d and u_{10} counteract each other to some degree and consequently yield similar wind stresses [cf. (1)] among the three flux parameterizations in the coupled runs (Fig. 7).

Since cases 4–6 yield similar evolutions of the simulated SST (cooling), only the results from CY16_C are analyzed in more detail. Figure 8 compares the CY16_C simulated SST with the TMI observed SST on 28 August; considerable agreement in both the distributions and magnitudes of SST (cooling) are evident. Therefore, it is concluded that the coupled model is capable of reproducing the ocean response during the TC passage.

As the TC simulated by CY16_C moved across the Gulf of Mexico, the SST decreased (first row of Fig. 7) and cold wakes were easily captured in the right-rear quadrant of the track [because of the near-resonant coupling of the wind stress and the wind driven near-inertial rotating velocity (Price 1981)]. The maximum SST cooling of up to 5°–6°C occur at around 24°N, 84°W and 28°N, 89°W, corresponding well with the cold core eddies shown in Fig. 4. Between these two locations, the simulated TCs traversed the Loop Current (during about 48–66 h after initialization), where SST never fell below 27°C. This warm core eddy likely contributed to TC intensification (Figs. 6b,d).

d. Time evolution of TC radial structure

Radius–time Hovmöller diagrams of azimuthally averaged fields are used to analyze the radial variability both within and between the simulated TCs during intensification and decay periods between 1200 UTC 26 August and 0000 UTC 30 August (12 and 96 h after initialization, respectively). Only the runs using momentum flux options CY16 or GZ13 are discussed here, because the results of WRF2 mostly fall in between them.

For the first 90 h of the uncoupled runs (CY16_A and GZ13_A), the simulated TCs continued to intensify and expand in size (Figs. 9a,b). For the coupled runs (CY16_C and GZ13_C), $P_{\min}$ was minimized at around 66–72 h before the TCs encountered the cold core eddies, although the radii of 950-hPa isobar continued to expand outward until the TCs made landfall (Figs. 9c,d). In terms of 10-m winds, the larger difference between momentum flux options lies in the tangential direction, with larger C_d resulting in weaker tangential winds (Figs. 9e–h). This can also be seen in Fig. 10, which compares the inflow angles of CY16_C and GZ13_C at 0000 UTC 29 August. In the areas with 10-m winds above 40 m s^{-1} (i.e., the wind speeds at which C_d are most different between the different flux options; Fig. 1a) it can be seen that GZ13_C, with higher C_d than

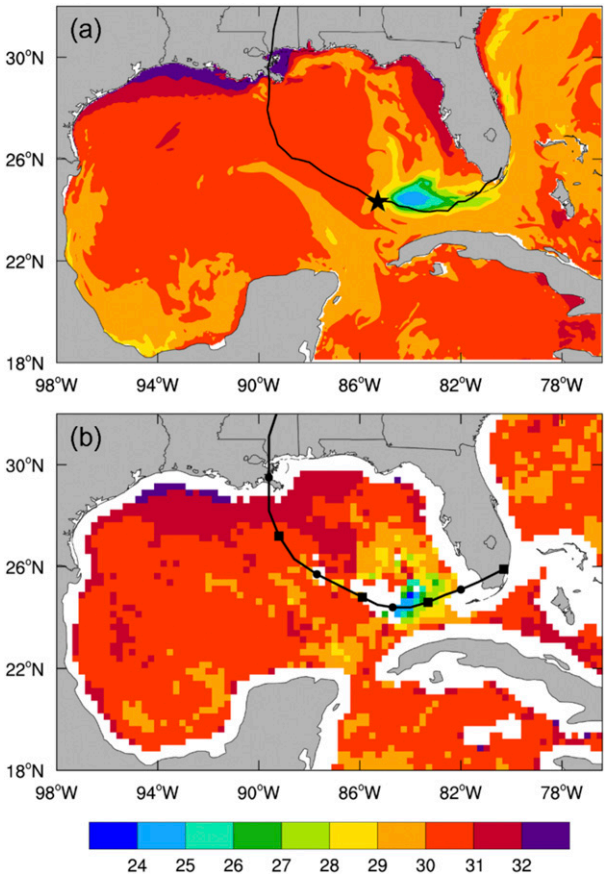

FIG. 8. (a) Distribution of SST (°C) for CY16_C at 0000 UTC 28 Aug 2005. The black line and the asterisk represent the simulated track and the position of the TC center at 0000 UTC 28 Aug, respectively. (b) Faster contours of TMI SST (°C) on 26–28 Aug 2005. Katrina's observed track is plotted as in Fig. 5.

CY16_C, also generally has a larger inflow angle. While it may be tempting to compare the simulation results to observations such as those presented in Zhang and Uhlhorn (2012), such a comparison would be better saved for a much larger number of runs in future studies rather than the case study here.

No firm conclusions can be drawn regarding the impact of changing C_d (at high wind speeds only) on the radius of maximum wind (RMW) at a height of 10 m (Figs. 9e–h). In Green and Zhang (2014), a much larger sample of uncoupled runs found that increasing C_d (for *all* wind speeds) yielded a decrease in RMW (their Figs. 4b,d), likely because higher C_d further disrupts gradient wind balance, allowing low-level inflow to get closer to the TC center (Smith et al. 2014). What Green and Zhang (2014) did not show was a corresponding plot to their Figs. 4b and 4d but for the m parameter (which only changed C_d at hurricane-force wind speeds, similar to the various C_d parameterizations tested here). Such a

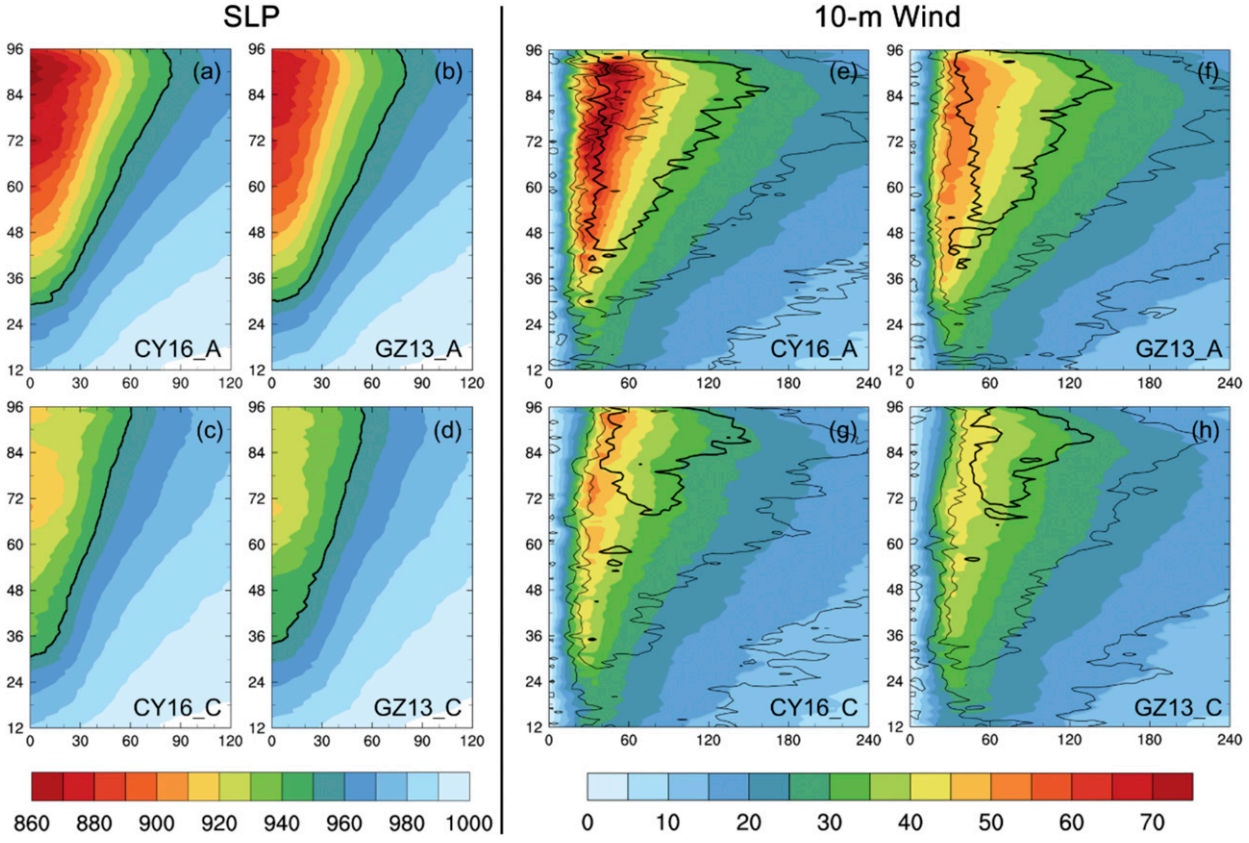

FIG. 9. Hovmöller diagrams of azimuthally averaged (left) SLP (hPa; the 950-hPa isobar shown by thick black lines) and (right) 10-m tangential winds (colors; m s^{-1}) and radial winds (black lines, contoured every 5 m s^{-1} with the thick line for the 15 m s^{-1} isotach). (a),(e) CY16_A; (b),(f) GZ13_A; (c),(g) CY16_C; (d),(h) GZ13_C. The *x* axis and *y* axis denote, respectively, distance (km) from TC center and hours since 0000 UTC 26 Aug 2005.

plot (not shown) indicated some evidence that increasing C_d only at high wind speeds could lead to a decrease in the RMW, but only for very strong TCs. It should be noted that Bryan (2012, his Fig. 8) found from idealized axisymmetric atmosphere-only TC simulations that changing C_d (C_k was held fixed) generally had no impact on RMW, except in the case of a very large horizontal diffusion length scale (l_h = 3 km). Given the very different experimental setups between Bryan (2012) and the present work [which is much closer to Green and Zhang (2014) than to Bryan (2012)], the most that can be said here is that a determination of the impact (if any) of C_d on the RMW would require hundreds of experiments following Green and Zhang (2014) but for coupled simulations. Nevertheless, it is not surprising to see in Figs. 9e–h that a decreased C_d at high wind speeds (CY16) yields a stronger radial gradient in the tangential wind field near the eyewall: this is a direct consequence of the CY16 runs having stronger winds than the GZ13 runs near the RMW, but similar winds at larger radii (e.g., ~120–150 km). This is true for both the uncoupled and coupled runs. Obviously, extending the study of Green and Zhang (2014)—with a much larger sample size—to coupled runs would yield more conclusive results.

Radius–time plots of $\Delta\theta$, H_S, ΔQ, and H_L are shown in Figs. 11–14, respectively, for the uncoupled [CY16_A and GZ13_A; panels (a) and (e), respectively] and coupled runs [CY16_C and GZ13_C; panels (b) and (f), respectively]. The latent heat flux is found to be the dominant factor in the moist enthalpy transfer across the air–sea interface in these TC simulations. Field measurements (e.g., Zhang et al. 2008) also support this finding. GZ13_A has higher sensible and latent heat fluxes than those in CY16_A due to larger C_h and C_q and larger differences in temperature ($\Delta\theta$) and water vapor (ΔQ) between the sea surface and the air immediately above. However, CY16_A—despite lower surface heat fluxes than GZ13_A—has lower sea level pressures (Figs. 6a and 9a,b), which is different from the findings of Green and Zhang (2013). It should be noted that Green and Zhang (2014, their Figs. 3a,c) showed no statistically

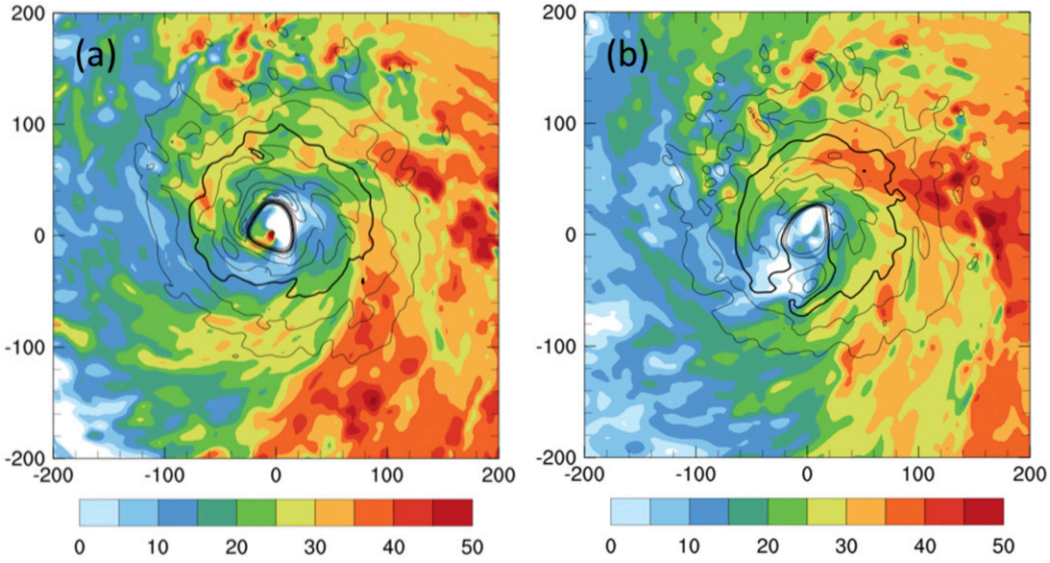

FIG. 10. Inflow angles in degrees (color) and wind speeds (black lines, contoured every 5 m s^{-1} from 30 m s^{-1} with the thick line for the 40 m s^{-1} isotach) at a height of 10 m simulated by (a) CY16_C and (b) GZ13_C, valid at 0000 UTC 29 Aug 2005.

significant correlation between the slope of C_d at hurricane-force wind speeds (their experimental parameter m) and $P_{\min}$. While not possible with the available model output, an energy budget analysis following Wang and Xu (2010) might be able to shed insight as to why CY16_A has lower pressures than GZ13_A despite smaller surface heat fluxes. In the coupled runs the enthalpy (both sensible and latent heat) fluxes become much closer between GZ13 and CY16 because of the similar $\Delta\theta$ and ΔQ. The enthalpy

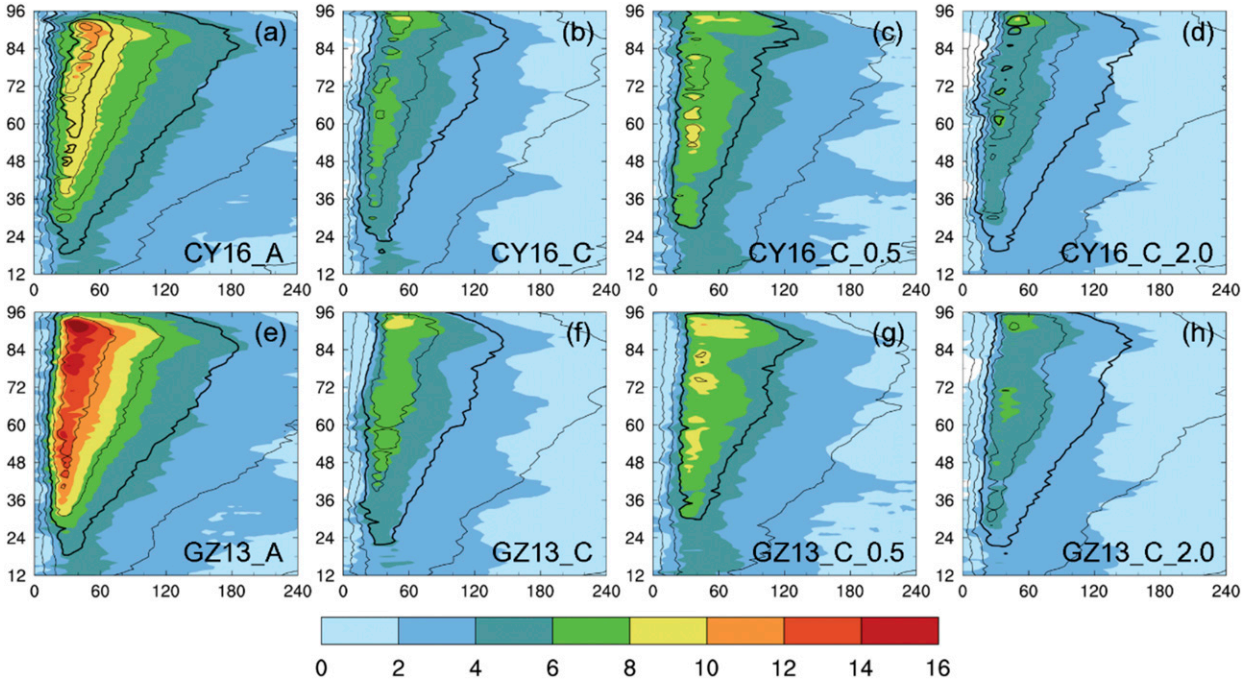

FIG. 11. Hovmöller diagrams of azimuthally averaged $\Delta\theta$ (colors; K) and 10-m wind speed (black lines, contoured every 10 m s^{-1} with the thick lines for 30 and 60 m s^{-1} isotachs). (a) CY16_A with $\beta = 1.0$; (b)–(d) CY16_C with $\beta = 1.0$, 0.5, and 2.0, respectively; (e) GZ13_A; and (f)–(h) GZ13_C with $\beta = 1.0$, 0.5, and 2.0, respectively. The x axis and y axis are as in Fig. 9.

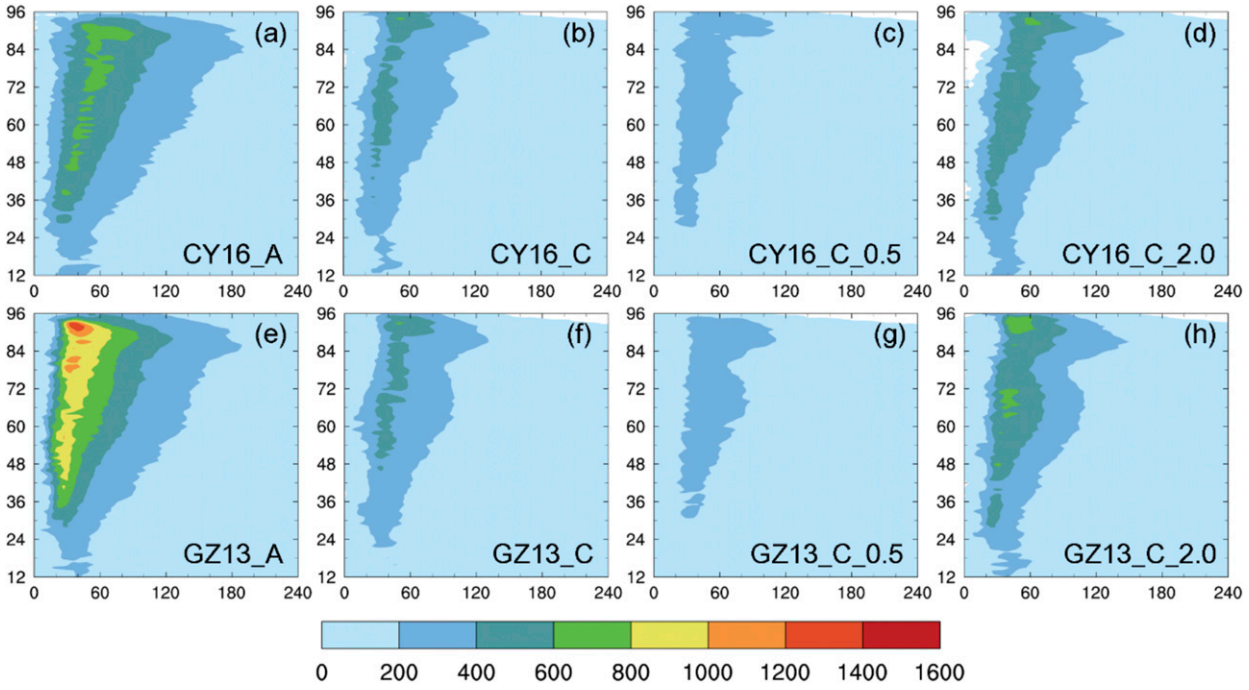

FIG. 12. As in Fig. 11, but for surface flux of sensible heat ($W\,m^{-2}$).

fluxes in the coupled runs are lower than their corresponding uncoupled runs, which is mainly attributed to the smaller $\Delta\theta$ and ΔQ caused by SST cooling, and weaker wind speeds (Figs. 11a,b,e,f and Figs. 13a,b,e,f).

Additionally, it is evident in Figs. 14b,f that latent heat flux for the coupled runs (cases 4–6) had a local maximum between 48 and 72 h (this was also true for WRF2_C, but is not shown here). During that period, Katrina traversed the Loop Current where the oceanic heat content values were large (Jaimes and Shay 2009) and the ocean cooled less in response (Fig. 7). Therefore, all three coupled runs intensified in terms of pressure deepening (Fig. 6b), which was also observed in the best track. This again indicates that numerical forecasts of TC intensity should take the mesoscale oceanic variability into account, which can only be achieved by the approach of three-dimensional atmosphere–ocean two-way coupled modeling. However, CY16_C is the only case that was able to successfully capture the observed increase in V_{max}, which is possibly because C_d is lower in this run.

e. *Sensitivity to moist enthalpy parameterization*

To further examine the sensitivity of simulated TC intensity to the uncertainty in C_k, the simulated P_{min} and V_{max} from cases 4–18 (all of which are atmosphere–ocean coupled runs) are shown in Fig. 15 along with the corresponding C_h curves [as stated above, because (10) and (11) yield nearly identical curves of C_h and C_q for a given C_d, either heat exchange coefficient is essentially the same as C_k]. Moreover, recall from section 2b that increasing β generally increases C_k (except for when u_{10} exceeds about $70\,m\,s^{-1}$, β has little impact on the CY16-derived C_k). Generally speaking for all three momentum flux parameterizations, increasing β yields more intense simulated TCs in terms of both P_{min} and V_{max}, which is consistent with the results of sensitivity tests to β conducted in Green and Zhang (2014) for uncoupled (atmosphere only) simulations.

While CY16_C ($\beta = 1.0$) appears to give the most consistent result with the best track observation, the huge spread of P_{min} and V_{max} associated with changing β in the CY16 framework deserves more attention: if a decrease in C_d at very strong winds is what actually happens in nature, then C_k becomes even more important for forecasts. However, for the cases with the momentum flux options WRF2 and GZ13, although a large spread is still evident in terms of P_{min}, the value of C_k matters much less for V_{max}. It is also interesting to note that the general pattern of higher β yielding a more intense TC does not hold when β is increased from 1.5 to 2.0 for these two options; whether this is due to random chance or indicative of a more physically based process is beyond the scope of this paper. Moreover, none of the WRF2 or GZ13 simulations predict a peak V_{max} that is comparable to the best track: they all underestimate the observed TC intensity.

As a whole, the impacts of both C_d and C_k on the pressure–wind relationships (for coupled runs) are

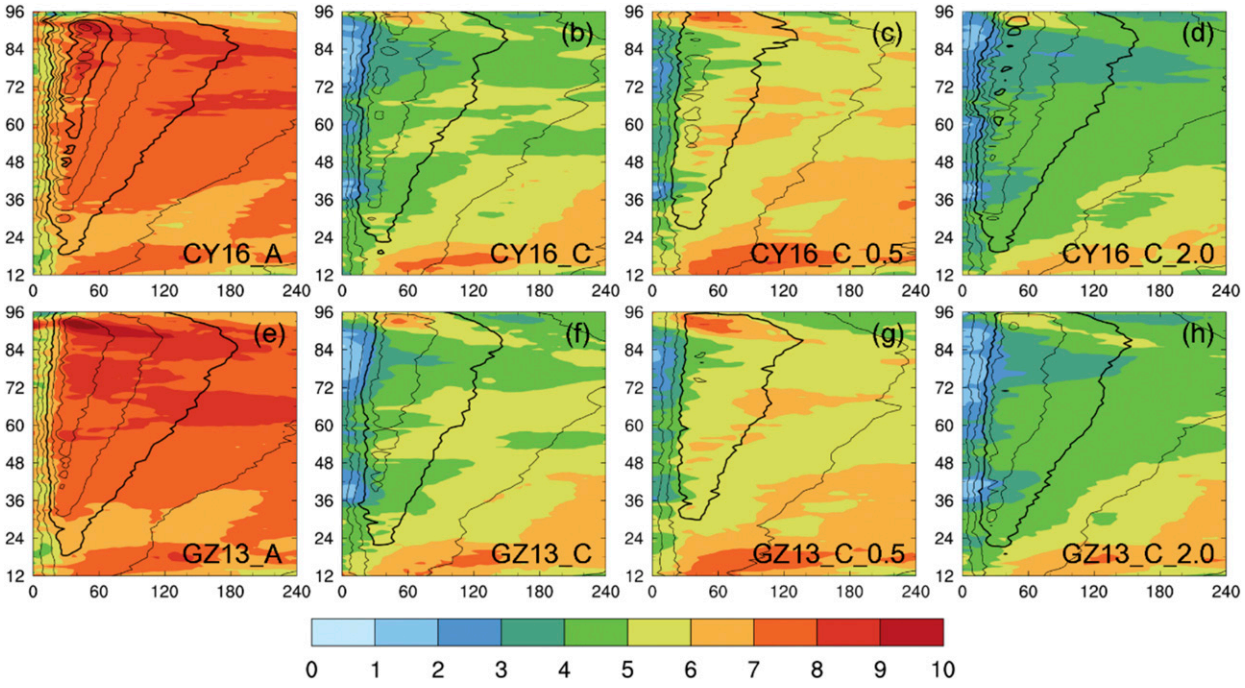

FIG. 13. As in Fig. 11, but for ΔQ (colors; g kg^{-1}) and 10-m wind speed (black lines, contoured every 10 m s^{-1} with the thick lines for 30 and 60 m s^{-1} isotachs).

plotted in Fig. 16. Results show that the relationship does not vary much due to β (i.e., C_k alone), consistent with Green and Zhang (2014). But, changing the behavior of C_d at extreme wind speeds (i.e., CY16, WRF2, and GZ13) does change the slope of these best-fit lines in the way that the uncoupled runs in Green and Zhang (2013, 2014) also showed: increasing C_d (blue to green to red) deepens $P_{\min}$ (for a given $V_{\max}$).

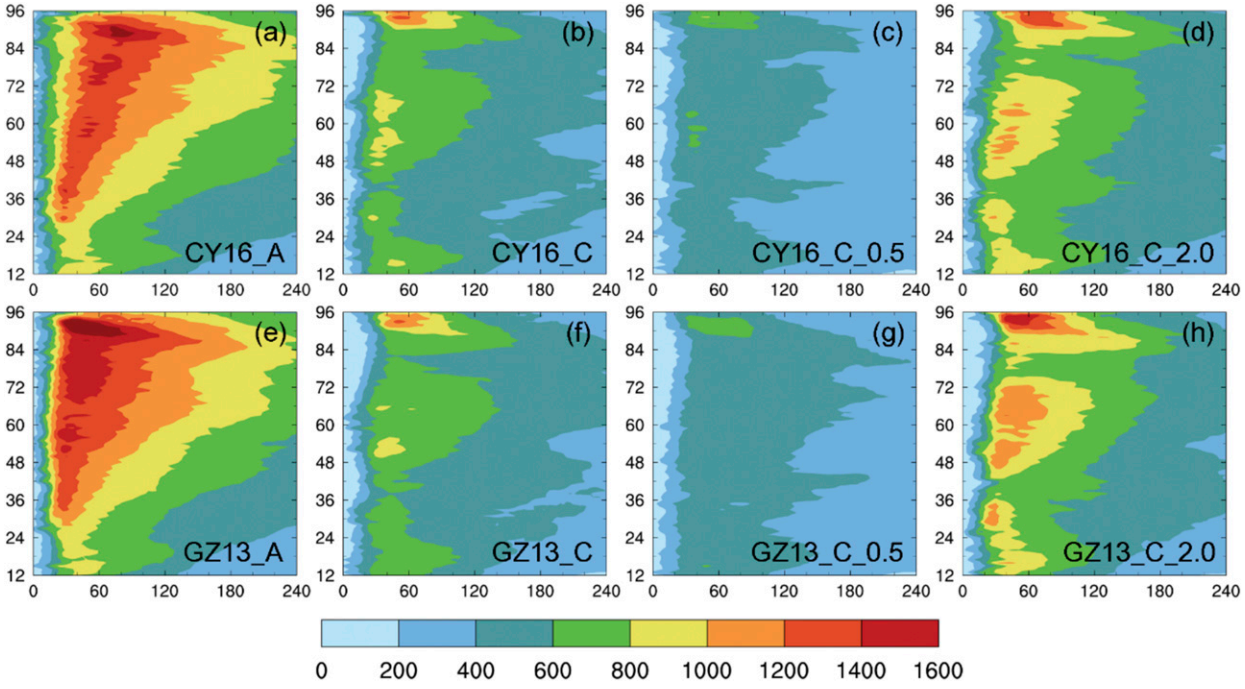

FIG. 14. As in Fig. 12, but for surface flux of latent heat (W m^{-2}).

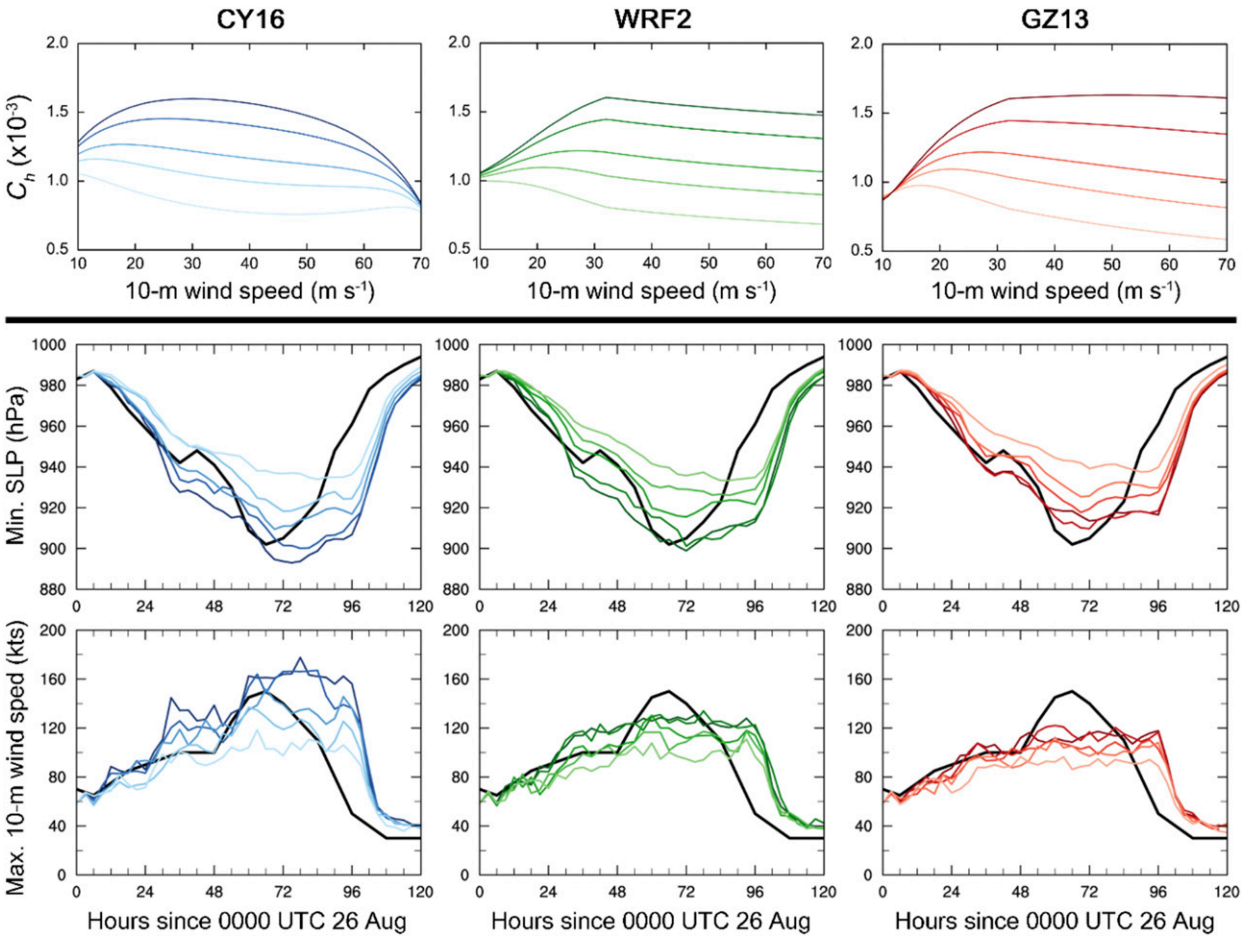

FIG. 15. Sensitivity experiments testing the impact of uncertainty in moist enthalpy flux parameterization. (top) Exchange coefficient of sensible heat C_h [calculated via (10)] as a function of 10-m wind speed, for each of the three momentum flux parameterizations. The sensitivity of C_h to the β parameter in (10) is shown for $\beta = 0.5, 0.75, 1.0, 1.5$, and 2.0, with darker colors indicating a higher value of β. The temporal evolutions of (middle) minimum SLP and (bottom) maximum 10-m wind speed for the simulated TCs corresponding to these flux parameterization changes (cf. cases 4–18 in Table 1) are shown in the same color pattern. The observed best track intensity of Katrina is also shown in black in the bottom two rows.

The sensitivity of heat fluxes to the value of β (i.e., C_k) is also shown in Figs. 11–14. Increased β (e.g., CY16_C_2.0 and GZ13_C_2.0) reduces $\Delta\theta$ and ΔQ across the air–sea interface, but the resulting sensible and latent heat fluxes still increase because of the larger C_k and stronger surface winds. Decreased β (e.g., CY16_C_0.5 and GZ13_C_0.5) yields the opposite results. Thus, there is a positive correlation between β (C_k), heat flux, and surface winds. However, this relationship is no longer valid for flux options WRF2 and GZ13 if β exceeds a relatively large value (i.e., $\beta > 1.5$).

5. Conclusions

Accurate forecasts of tropical cyclones (TCs) are of great significance, so that the losses caused by these disastrous storms can be minimized. Although TC track forecasts have substantially improved over time, skillfully predicting TC intensity remains elusive. Previous studies have shown that simulated TC intensity is quite sensitive to momentum and moist enthalpy fluxes across the air–sea interface. But how the drag coefficient C_d actually behaves in high wind conditions over the ocean still remains uncertain. Because TCs can induce SST cooling that acts as a negative feedback process against continuous intensification, there has been a concerted effort in recent years to simulate TCs in a coupled atmosphere–ocean modeling framework.

This study uses COAWST, which couples the atmospheric WRF Model with the three-dimensional oceanic ROMS model, to investigate the combined impacts of TC-induced SST cooling and momentum flux

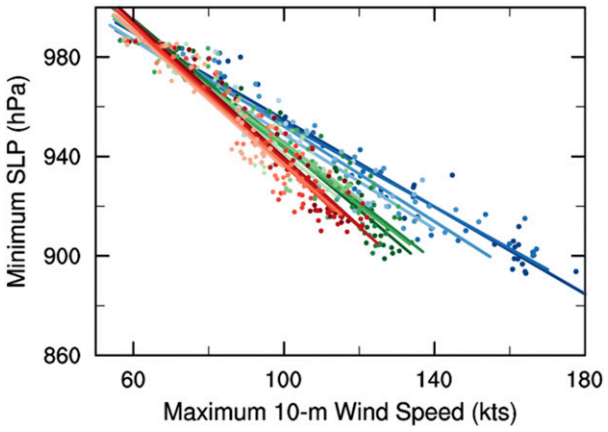

FIG. 16. Pressure–wind relationship yielded by CY16_C (blue), WRF2_C (green), and GZ13_C (red) with different β (= 0.5, 0.75, 1.0, 1.5, 2.0) in (10) and (11). The circles mark 3-hourly output and the straight lines represent the best fit of each case. The darker colors correspond to larger β.

parameterizations on the intensity and structure of Hurricane Katrina. Three parameterizations for momentum flux—which represent increasing, steady, or decreasing C_d for 10-m wind speeds greater than $\sim$33 m s^{-1}—are chosen. The sensitivity of hurricane intensity to the parametric uncertainty in moist enthalpy exchange coefficient C_k is also examined. The major conclusions from this research are as follows.

Near-surface (10 m) wind speeds largely depend on the surface momentum flux option, though the SLP and TC track are less sensitive to it. As conjectured in Green and Zhang (2014, p. 2305), an explanation as to why changing C_d *only at hurricane-force winds* (which is essentially the difference in the C_d parameterizations tested in this study) yields more significant changes to V_{max} than to P_{min} is that the former metric is directly impacted by C_d: for a given radial pressure gradient (assuming near-gradient-wind balance in the free atmosphere), increasing C_d will directly decrease the 10-m wind speeds (including V_{max}) *diagnosed* by the surface layer scheme. In contrast, P_{min} is a reflection of both angular momentum dynamics and warm-core thermodynamics. While Green and Zhang (2014) stated that increased surface heat fluxes (which can be obtained by increasing C_d and thus C_k) could lead to decreases in P_{min}, it was found here that in uncoupled runs, flux option GZ13, with higher C_d at hurricane-force wind speeds than flux option CY16, had *higher* values of P_{min} than CY16 despite stronger surface heat fluxes (Figs. 6a; 9a,b; 11a,e; and 13a,e). But it is important to remember that Green and Zhang (2014) also showed no statistically significant relationship between changing C_d *at hurricane-force wind speeds only* and P_{min}. A more detailed investigation into the dynamics of how C_d impacts P_{min} is beyond the scope of the present study, but it is safe to say that the relationship between C_d and V_{max} is much more straightforward than the relationship between C_d and P_{min}.

The flux option CY16, which at hurricane-force wind speeds has both the smallest C_d and the largest C_k/C_d, produces the most intense TC—particularly for maximum 10-m wind speed V_{max}. The simulated TCs in the coupled runs (which can consider SST cooling) are less intense than the uncoupled runs with time-fixed SST. The coupled run using the CY16 flux parameterization yields temporal evolutions of both P_{min} and V_{max} that are in best agreement with the observations.

All three coupled runs (with changes to C_k only caused by changes to C_d) have similar temporal evolutions of SST that are consistent with satellite observations. Their simulated TCs underwent intensification (decay) when traversing the warm core Loop Current (cold core eddies), and the maximum SST reductions of up to 6°–7°C occurred at the locations of the cold core oceanic eddies. Both of these results indicate that mesoscale oceanic variability can be of critical importance for TC-induced SST cooling, and consequently impact TC intensity. Therefore, it is suggested that TC numerical prediction systems be coupled with a three-dimensional ocean model in order to obtain more accurate intensity forecasts.

In coupled runs, increased C_k increases the heat fluxes across the air–sea interface (despite reducing air–sea differences in temperature and moisture) and consequently yields more intense simulated TCs. If a decrease in C_d at very strong winds (like CY16) is what actually happens in nature, then C_k becomes even more important for forecasts; that is, the TC intensity is extremely sensitive to C_k in this circumstance. On the other hand, the simulations of Hurricane Katrina with WRF2 and GZ13 always underestimate V_{max} regardless of the magnitude of C_k.

Within the atmosphere–ocean coupled model framework, using a momentum flux parameterization that allows C_d to decrease at extreme hurricane-force wind speeds with the default C_k scheme is shown to improve the accuracy of TC intensity forecasts for simulations of Hurricane Katrina (2005). A reduced C_d at extreme wind speeds over the ocean is supported in field observations from several studies (e.g., Powell et al. 2003; Jarosz et al. 2007; Holthuijsen et al. 2012).

Future work is needed to address the limitations of the present study. First and foremost, the dissipative heating term—which was included here—might introduce a spurious source of energy and should not be included (computational constraints prevented us from redoing all of the experiments with dissipative heating

turned off). Second, a much larger sample size—either through a more systematic variation of C_d and C_k as in Green and Zhang (2014) but for a coupled model, or through many more TC cases—is necessary to draw more firm conclusions. Third, surface flux parameterization sensitivity studies would benefit greatly from further coupling to a surface wave model that calculates the wave-dependent wind stress, using the methods such as in Chen and Yu (2016, 2017). Fourth, a more thorough analysis of TC structure—including comparisons with observations—would provide valuable insight. And finally, the overall robustness of the results (i.e., how the *general* conclusions of this work are impacted) to changes in other physics parameterizations, particularly for the planetary boundary layer, should be tested.

Acknowledgments. Yingjian Chen and Xiping Yu are financially supported by National Natural Science Foundation of China (NSFC) under Grant 11732008 and by State Key Laboratory of Hydroscience and Engineering, China, under Grant 2014-KY-02. Yingjian Chen is also supported by China Scholarship Council (CSC). Fuqing Zhang is supported by NOAA under the Hurricane Forecast Improvement Program (HFIP) and the Office of Naval Research under Grant N000140910526. Benjamin W. Green is supported by NOAA under Award NA17OAR4320101. The authors would also like to thank John C. Warner for his publically available model COAWST. The computing was performed at the Texas Advanced Computing Center (TACC). All data used in this study are stored on TACC and are available upon request from the authors. The authors also thank the editor Dr. Ron McTaggart-Cowan and two anonymous reviewers for their comments, which substantially improved the quality of this manuscript.

REFERENCES

Andreas, E. L, 2004: Spray stress revisited. *J. Phys. Oceanogr.*, **34**, 1429–1440, https://doi.org/10.1175/1520-0485(2004)034<1429:SSR>2.0.CO;2.

Booij, N., R. C. Ris, and L. H. Holthuijsen, 1999: A third-generation wave model for coastal regions—1. Model description and validation. *J. Geophys. Res.*, **104**, 7649–7666, https://doi.org/10.1029/98JC02622.

Brutsaert, W., 1975: A theory for local evaporation (or heat transfer) from rough and smooth surfaces at ground level. *Water Resour. Res.*, **11**, 543–550, https://doi.org/10.1029/WR011i004p00543.

Bryan, G. H., 2012: Effects of surface exchange coefficients and turbulence length scales on the intensity and structure of numerically simulated hurricanes. *Mon. Wea. Rev.*, **140**, 1125–1143, https://doi.org/10.1175/MWR-D-11-00231.1.

Chapman, D. C., 1985: Numerical treatment of cross-shelf open boundaries in a barotropic coastal ocean model. *J. Phys. Oceanogr.*, **15**, 1060–1075, https://doi.org/10.1175/1520-0485(1985)015<1060:NTOCSO>2.0.CO;2.

Chen, S., T. J. Campbell, H. Jin, S. Gaberšek, R. M. Hodur, and P. Martin, 2010: Effect of two-way air–sea coupling in high and low wind speed regimes. *Mon. Wea. Rev.*, **138**, 3579–3602, https://doi.org/10.1175/2009MWR3119.1.

Chen, S. S., J. F. Price, W. Zhao, M. A. Donelan, and E. J. Walsh, 2007: The CBLAST-Hurricane program and the next-generation fully coupled atmosphere–wave–ocean models for hurricane research and prediction. *Bull. Amer. Meteor. Soc.*, **88**, 311–317, https://doi.org/10.1175/BAMS-88-3-311.

Chen, Y., and X. Yu, 2016: Enhancement of wind stress evaluation method under storm conditions. *Climate Dyn.*, **47**, 3833–3843, https://doi.org/10.1007/s00382-016-3044-4.

——, and ——, 2017: Sensitivity of storm wave modeling to wind stress evaluation methods. *J. Adv. Model. Earth Syst.*, **9**, 893–907, https://doi.org/10.1002/2016MS000850.

Davis, C., and Coauthors, 2008: Prediction of landfalling hurricanes with the Advanced Hurricane WRF Model. *Mon. Wea. Rev.*, **136**, 1990–2005, https://doi.org/10.1175/2007MWR2085.1.

Donelan, M. A., F. W. Dobson, S. D. Smith, and R. J. Anderson, 1993: On the dependence of sea surface roughness on wave development. *J. Phys. Oceanogr.*, **23**, 2143–2149, https://doi.org/10.1175/1520-0485(1993)023<2143:OTDOSS>2.0.CO;2.

——, B. K. Haus, N. Reul, W. J. Plant, M. Stiassnie, H. C. Graber, O. B. Brown, and E. S. Saltzman, 2004: On the limiting aerodynamic roughness of the ocean in very strong winds. *Geophys. Res. Lett.*, **31**, L18306, https://doi.org/10.1029/2004GL019460.

Dudhia, J., 1989: Numerical study of convection observed during the Winter Monsoon experiment using a mesoscale two-dimensional model. *J. Atmos. Sci.*, **46**, 3077–3107, https://doi.org/10.1175/1520-0469(1989)046<3077:NSOCOD>2.0.CO;2.

Emanuel, K. A., 1995: Sensitivity of tropical cyclones to surface exchange coefficients and a revised steady-state model incorporating eye dynamics. *J. Atmos. Sci.*, **52**, 3969–3976, https://doi.org/10.1175/1520-0469(1995)052<3969:SOTCTS>2.0.CO;2.

Flather, R. A., 1976: A tidal model of the northwest European continental shelf. *Mem. Soc. Roy. Sci. Liège*, **10**, 141–164.

Garratt, J. R., 1977: Review of drag coefficients over oceans and continents. *Mon. Wea. Rev.*, **105**, 915–929, https://doi.org/10.1175/1520-0493(1977)105<0915:RODCOO>2.0.CO;2.

——, 1992: *The Atmospheric Boundary Layer.* Cambridge University Press, 316 pp.

Glenn, S. M., and Coauthors, 2016: Stratified coastal ocean interactions with tropical cyclones. *Nat. Commun.*, **7**, 10887, https://doi.org/10.1038/ncomms10887.

Green, B. W., and F. Zhang, 2013: Impacts of air–sea flux parameterizations on the intensity and structure of tropical cyclones. *Mon. Wea. Rev.*, **141**, 2308–2324, https://doi.org/10.1175/MWR-D-12-00274.1.

——, and ——, 2014: Sensitivity of tropical cyclone simulations to parametric uncertainties in air–sea fluxes and implications for parameter estimation. *Mon. Wea. Rev.*, **142**, 2290–2308, https://doi.org/10.1175/MWR-D-13-00208.1.

Grell, G. A., and D. Devenyi, 2002: A generalized approach to parameterizing convection combining ensemble and data assimilation techniques. *Geophys. Res. Lett.*, **29**, https://doi.org/10.1029/2002GL015311.

Halliwell, G. R., S. Gopalakrishnan, F. Marks, and D. Willey, 2015: Idealized study of ocean impacts on tropical cyclone intensity forecasts. *Mon. Wea. Rev.*, **143**, 1142–1165, https://doi.org/10.1175/MWR-D-14-00022.1.

Holthuijsen, L. H., M. D. Powell, and J. D. Pietrzak, 2012: Wind and waves in extreme hurricanes. *J. Geophys. Res.*, **117**, C09003, https://doi.org/10.1029/2012JC007983.

Hong, S., and J. J. Lim, 2006: The WRF single-moment 6-class microphysics scheme (WSM6). *J. Korean Meteor. Soc.*, **42**, 129–151.

——, Y. Noh, and J. Dudhia, 2006: A new vertical diffusion package with an explicit treatment of entrainment processes. *Mon. Wea. Rev.*, **134**, 2318–2341, https://doi.org/10.1175/MWR3199.1.

Jaimes, B., and L. K. Shay, 2009: Mixed layer cooling in mesoscale oceanic eddies during Hurricanes Katrina and Rita. *Mon. Wea. Rev.*, **137**, 4188–4207, https://doi.org/10.1175/2009MWR2849.1.

Jarosz, E., D. A. Mitchell, D. W. Wang, and W. J. Teague, 2007: Bottom-up determination of air-sea momentum exchange under a major tropical cyclone. *Science*, **315**, 1707–1709, https://doi.org/10.1126/science.1136466.

Jones, P. W., 1998: A users guide for SCRIP: A spherical coordinate remapping and interpolation package, version 1.4. Los Alamos National Laboratory, 29 pp.

Kilic, C., and C. C. Raible, 2013: Investigating the sensitivity of hurricane intensity and trajectory to sea surface temperatures using the regional model WRF. *Meteor. Z.*, **22**, 685–698, https://doi.org/10.1127/0941-2948/2013/0472.

Knabb, R. D., J. R. Rhome, and D. P. Brown, 2006: Tropical cyclone report: Hurricane Katrina (23–30 August 2005). NOAA/NHC Rep. AL122005, 43 pp., http://www.nhc.noaa.gov/data/tcr/AL122005_Katrina.pdf.

Kudryavtsev, V. N., 2006: On the effect of sea drops on the atmospheric boundary layer. *J. Geophys. Res.*, **111**, C07020, https://doi.org/10.1029/2005JC002970.

——, and V. K. Makin, 2011: Impact of ocean spray on the dynamics of the marine atmospheric boundary layer. *Bound.-Layer Meteor.*, **140**, 383–410, https://doi.org/10.1007/s10546-011-9624-2.

Large, W. G., and S. Pond, 1981: Open ocean momentum flux measurements in moderate to strong winds. *J. Phys. Oceanogr.*, **11**, 324–336, https://doi.org/10.1175/1520-0485(1981)011<0324:OOMFMI>2.0.CO;2.

Larson, J., R. Jacob, and E. Ong, 2005: The Model Coupling Toolkit: A new Fortran90 toolkit for building multiphysics parallel coupled models. *Int. J. High Perform. Comput. Appl.*, **19**, 277–292, https://doi.org/10.1177/1094342005056115.

Mei, W., C. Lien, I. I. Lin, and S. Xie, 2015: Tropical cyclone–induced ocean response: A comparative study of the South China Sea and tropical northwest Pacific. *J. Climate*, **28**, 5952–5968, https://doi.org/10.1175/JCLI-D-14-00651.1.

Mlawer, E. J., S. J. Taubman, P. D. Brown, M. J. Iacono, and S. A. Clough, 1997: Radiative transfer for inhomogeneous atmospheres: RRTM, a validated correlated-k model for the longwave. *J. Geophys. Res.*, **102**, 16 663–16 682, https://doi.org/10.1029/97JD00237.

Moon, I., T. Hara, I. Ginis, S. E. Belcher, and H. L. Tolman, 2004: Effect of surface waves on air–sea momentum exchange: I. Effect of mature and growing seas. *J. Atmos. Sci.*, **61**, 2321–2333, https://doi.org/10.1175/1520-0469(2004)061<2321:EOSWOA>2.0.CO;2.

Olabarrieta, M., J. C. Warner, B. Armstrong, J. B. Zambon, and R. Y. He, 2012: Ocean-atmosphere dynamics during Hurricane Ida and Nor'Ida: An application of the coupled ocean-atmosphere-wave-sediment transport (COAWST) modeling system. *Ocean Modell.*, **43–44**, 112–137, https://doi.org/10.1016/j.ocemod.2011.12.008.

Powell, M. D., P. J. Vickery, and T. A. Reinhold, 2003: Reduced drag coefficient for high wind speeds in tropical cyclones. *Nature*, **422**, 279–283, https://doi.org/10.1038/nature01481.

Price, J. F., 1981: Upper ocean response to a hurricane. *J. Phys. Oceanogr.*, **11**, 153–175, https://doi.org/10.1175/1520-0485(1981)011<0153:UORTAH>2.0.CO;2.

Rappaport, E. N., and Coauthors, 2009: Advances and challenges at the National Hurricane Center. *Wea. Forecasting*, **24**, 395–419, https://doi.org/10.1175/2008WAF2222128.1.

Seo, H., and S. Xie, 2013: Impact of ocean warm layer thickness on the intensity of hurricane Katrina in a regional coupled model. *Meteor. Atmos. Phys.*, **122**, 19–32, https://doi.org/10.1007/s00703-013-0275-3.

Seroka, G., T. Miles, Y. Xu, J. Kohut, O. Schofield, and S. Glenn, 2016: Hurricane Irene sensitivity to stratified coastal ocean cooling. *Mon. Wea. Rev.*, **144**, 3507–3530, https://doi.org/10.1175/MWR-D-15-0452.1.

Shchepetkin, A. F., and J. C. McWilliams, 2005: The regional oceanic modeling system (ROMS): A split-explicit, free-surface, topography-following-coordinate oceanic model. *Ocean Modell.*, **9**, 347–404, https://doi.org/10.1016/j.ocemod.2004.08.002.

Skamarock, W. C., and Coauthors, 2008: A description of the Advanced Research WRF version 3. NCAR Tech. Note NCAR/TN-475+STR, 113 pp., https://dx.doi.org/10.5065/D68S4MVH.

Smith, R. K., M. T. Montgomery, and G. L. Thomsen, 2014: Sensitivity of tropical-cyclone models to the surface drag coefficient in different boundary-layer schemes. *Quart. J. Roy. Meteor. Soc.*, **140**, 792–804, https://doi.org/10.1002/qj.2057.

Tallapragada, V., and Coauthors, 2015: Hurricane Weather Research and Forecasting (HWRF) model: 2015 scientific documentation. NCAR Tech. Note NCAR/TN-522+STR, 122 pp., https://dtcenter.org/HurrWRF/users/docs/scientific_documents/HWRF_v3.7a_SD.pdf.

Taylor, P. K., and M. J. Yelland, 2001: The dependence of sea surface roughness on the height and steepness of the waves. *J. Phys. Oceanogr.*, **31**, 572–590, https://doi.org/10.1175/1520-0485(2001)031<0572:TDOSSR>2.0.CO;2.

Wang, Y., and J. Xu, 2010: Energy production, frictional dissipation, and maximum intensity of a numerically simulated tropical cyclone. *J. Atmos. Sci.*, **67**, 97–116, https://doi.org/10.1175/2009JAS3143.1.

Warner, J. C., C. R. Sherwood, H. G. Arango, and R. P. Signell, 2005: Performance of four turbulence closure models implemented using a generic length scale method. *Ocean Modell.*, **8**, 81–113, https://doi.org/10.1016/j.ocemod.2003.12.003.

——, ——, R. P. Signell, C. K. Harris, and H. G. Arango, 2008: Development of a three-dimensional, regional, coupled wave, current, and sediment-transport model. *Comput. Geosci.*, **34**, 1284–1306, doi:10.1016/j.cageo.2008.02.012.

——, B. Armstrong, R. Y. He, and J. B. Zambon, 2010: Development of a coupled ocean-atmosphere-wave-sediment transport (COAWST) modeling system. *Ocean Modell.*, **35**, 230–244, https://doi.org/10.1016/j.ocemod.2010.07.010.

Weng, Y., and F. Zhang, 2012: Assimilating airborne Doppler radar observations with an ensemble Kalman Filter for convection-permitting hurricane initialization and prediction: Katrina (2005). *Mon. Wea. Rev.*, **140**, 841–859, https://doi.org/10.1175/2011MWR3602.1.

——, and ——, 2016: Advances in convection-permitting tropical cyclone analysis and prediction through EnKF assimilation of reconnaissance aircraft observations. *J. Meteor. Soc. Japan*, **94**, 345–358, https://doi.org/10.2151/jmsj.2016-018.

Wu, J., 1982: Wind-stress coefficients over sea surface from breeze to hurricane. *J. Geophys. Res.*, **87**, 9704–9706, https://doi.org/10.1029/JC087iC12p09704.

Zambon, J. B., R. He, and J. C. Warner, 2014: Investigation of hurricane Ivan using the coupled ocean-atmosphere-wave-sediment transport (COAWST) model. *Ocean Dyn.*, **64**, 1535–1554, https://doi.org/10.1007/s10236-014-0777-7.

Zhang, F., and Y. Weng, 2015: Predicting hurricane intensity and associated hazards: A five-year real-time forecast experiment with assimilation of airborne Doppler radar observations. *Bull. Amer. Meteor. Soc.*, **96**, 25–33, https://doi.org/10.1175/BAMS-D-13-00231.1.

——, and K. A. Emanuel, 2016: On the role of surface fluxes and WISHE in tropical cyclone intensification. *J. Atmos. Sci.*, **73**, 2011–2019, https://doi.org/10.1175/JAS-D-16-0011.1.

Zhang, J. A., P. G. Black, J. R. French, and W. M. Drennan, 2008: First direct measurements of enthalpy flux in the hurricane boundary layer: The CBLAST results. *Geophys. Res. Lett.*, **35**, L14813, https://doi.org/10.1029/2008GL034374.

——, and E. W. Uhlhorn, 2012: Hurricane sea surface inflow angle and an observation-based parametric model. *Mon. Wea. Rev.*, **140**, 3587–3605, https://doi.org/10.1175/MWR-D-11-00339.1.

Zweers, N. C., V. K. Makin, J. W. de Vries, and G. Burgers, 2010: A sea drag relation for hurricane wind speeds. *Geophys. Res. Lett.*, **37**, L21811, https://doi.org/10.1029/2010GL045002.

——, ——, ——, and V. N. Kudryavtsev, 2015: The impact of spray-mediated enhanced enthalpy and reduced drag coefficients in the modelling of tropical cyclones. *Bound.-Layer Meteor.*, **155**, 501–514, https://doi.org/10.1007/s10546-014-9996-1.